https://doi.org/10.5194/egusphere-2026-5183
Preprint. Discussion started: 7 September 2026

Seasonal reversal of circulation in Qeqertarsuup Tunua (Disko Bay), Greenland

Linda Latuta[1], Jed E. Lenetsky[2,3], Elin Darelius[1], and Lars H. Smedsrud[1]

[1]Geophysical Institute, University of Bergen and Bjerknes Centre for Climate Research, Bergen, Norway
[2]Department of Atmospheric and Oceanic Sciences and Institute of Arctic and Alpine Research, University of Colorado, Boulder, Colorado, USA
[3]Department of Earth and Planetary Sciences, Harvard University, Cambridge, Massachusetts, USA

Correspondence: Linda Latuta (linda.latuta@uib.no)

Abstract. Qeqertarsuup Tunua (Disko Bay), located in West Greenland, is a highly productive ecosystem and a major site of glacier-ocean interaction with the Kangia (Ilulissat Icefjord), yet its circulation and the mechanisms governing its seasonal variability have not been previously investigated. An empirical orthogonal function (EOF) analysis of upper-ocean velocity from the GLORYS12 reanalysis (1993–2026) provides the first quantitative description of the bay's dominant circulation mode, EOF1, which explains 55.8% of the variance and is coherent through the upper $\sim$130 m. EOF1 reveals a seasonal reversal between a cyclonic regime, in which an intensified West Greenland Current establishes cyclonic circulation in the bay, and an anticyclonic regime, in which the flow within the bay reverses. The seasonal cycle accounts for 49.5% of the mode's variance, with the cyclonic regime prevailing from approximately May–June to November–December (with a peak in August), and the anticyclonic regime dominating in January–April. The alternation is consistent with a reversal of the along-shelf ocean surface stress forcing, strongly correlated with the circulation mode. The bay's circulation is, in turn, coherent with the West Greenland Current system at Davis Strait, where observed near-surface along-strait velocities flowing into Baffin Bay approximately double during the cyclonic regime and fall to near zero during the anticyclonic regime. Temperature transport towards the bay along the West Greenland shelf is an order of magnitude larger during the cyclonic regime than during the anticyclonic regime (+7.6 against +0.7 TW). Independent evidence from seven drifting-iceberg trajectories (June–July 2025) and an Argo float (June–October 2022) is qualitatively in line with these regimes. By governing the seasonal delivery of the warmest, fastest-flowing West Greenland shelf water into the bay, this circulation mode affects the bay's heat budget and the near-surface transport of freshwater, nutrients, and larvae that support the region's fisheries.

1 Introduction

Qeqertarsuup Tunua (Disko Bay) is a large semi-enclosed embayment on the western coast of Greenland that opens into Baffin Bay through a broad mouth approximately 150 km wide (Fig. 1). Its eastern margin is dominated by interaction with the Kangia (Ilulissat Icefjord), the fjord where Sermeq Kujalleq, one of the most prolific glaciers of the Greenland Ice Sheet, resides (Joughin et al., 2004; Holland et al., 2008; Motyka et al., 2011; Khazendar et al., 2019; Joughin et al., 2020; Picton et al., 2025). Meltwater and icebergs exported from the bay entrain into the West Greenland Current system, thereby contributing to

https://doi.org/10.5194/egusphere-2026-5183
Preprint. Discussion started: 7 September 2026

freshwater fluxes into Baffin Bay and the Labrador Sea (Schiller-Weiss et al., 2024). Despite its oceanographic importance, the circulation of Qeqertarsuup Tunua remains poorly characterised, and the dynamical mechanisms controlling its seasonal variability have not been investigated.

The regional context is set by the large-scale circulation of Baffin Bay. The northward-flowing West Greenland boundary current system comprises a West Greenland Coastal Current (WGCC), which carries meltwater-laden coastal waters, and a West Greenland Current (WGC). WGC is a shelfbreak jet which transports cool, fresh Polar-origin waters (West Greenland Shelf Water) above the warm, saline Atlantic-origin waters (West Greenland Irminger Waters) that enter Baffin Bay through Davis Strait and subduct beneath the Polar-origin layer, propagating northward as a bottom-intensified current (Tang et al., 2004; Curry et al., 2011, 2014; Münchow et al., 2015; Gou et al., 2022; Huang et al., 2024). North of Davis Strait, the WGC and WGCC are less clearly delineated than nearer the southern tip of Greenland, where the flow structure is itself highly variable and not always coherent (Gou et al., 2022; Foukal and Pickart, 2023; Nelson et al., 2025). Thus, we refer to the combined system WGC/WGCC as a northward-flowing shelf and/or shelfbreak current throughout this study, mainly referring to it as WGC for consistency with previous studies focusing on Qeqertarsuup Tunua. On the western side of the bay, the southward-flowing Baffin Island Current (BIC) returns comparatively cold, fresh Arctic-origin waters (Tang et al., 2004; Pacini et al., 2020; Huang et al., 2024). Exchange between the WGC and the continental shelf, and hence with Qeqertarsuup Tunua, is strongly controlled by topography (Gladish et al., 2015a, b; Nelson et al., 2025; Huang et al., 2025): the Egedesminde Dyb trough (300–900 m deep) cuts across the shelf and provides the primary pathway for dense, warm waters into the bay, though this inflow is partially obstructed by the Egedesminde Dyb Sill at approximately 300 m depth (Gladish et al., 2015a; Latuta et al., 2025).

Within the upper 200 m, Qeqertarsuup Tunua's connection to Baffin Bay is not limited by bathymetry, meaning that both large-scale oceanic and atmospheric forcing can directly influence conditions inside the bay. Nevertheless, currents in Qeqertarsuup Tunua remain largely unobserved, with limited studies focusing on the circulation within the bay. The earliest general descriptions of flow in the bay were provided by Nielsen (1928) and Kiilerich (1943), who noted a weak eastward diversion of the WGC into the southern part of the bay, with westward outflow along the south coast of Disko Island. A more systematic investigation by Andersen (1981) described the general surface circulation as cyclonic, with subsurface eastward inflow of WGC waters along the southern boundary of the bay from May to September, northward flow past Ilulissat, and outflow northward through Sullorsuaq Strait (Vaigat Strait) and westward flow along the south coast of Disko Island (Fig. 1). Wintertime circulation in the bay is unobserved; however, visual observations of iceberg drift in Andersen (1981) were broadly consistent with westward flow south of Disko Island. Smith et al. (1937) suggested that approximately one-third of the WGC transport entering the Egedesminde Dyb trough diverted into the bay, while the remainder either crossed over the trough and joined the outflow south of Disko Island or recirculated as an eddy within the trough itself. More recently, Beaird et al. (2017) identified a narrow, northward-flowing current of glacially modified waters exiting Kangia in August, consistent with model results and patterns of elevated chlorophyll concentrations observed in remote sensing data (Wood et al., 2025).

Despite these earlier descriptions, key aspects of Qeqertarsuup Tunua's circulation variability, including its seasonality, dominant dynamical modes, and relationship to large-scale atmospheric and oceanic forcing, remain uninvestigated. The ob-

https://doi.org/10.5194/egusphere-2026-5183
Preprint. Discussion started: 7 September 2026

servational record in the region is heavily biased towards the summer months, and the absence of in situ velocity measurements within the bay means that even the basic picture of cyclonic flow described by the aforementioned studies has not been quantitatively validated.

Ocean reanalysis products offer a route to characterise the three-dimensional circulation of Qeqertarsuup Tunua continuously over multi-decadal periods. While reanalyses necessarily involve model assumptions and must be used with caution in coastal regions and areas with complex topography, they provide the temporal and spatial coverage that in-situ observations alone cannot achieve, and have been shown to capture the broad structure of Baffin Bay circulation when compared against sparse mooring and shipboard data (Huang et al., 2024).

Here, we use the Global Ocean Physics Reanalysis (GLORYS12) product to characterise the dominant mode of circulation variability in Qeqertarsuup Tunua using empirical orthogonal function (EOF) analysis. We identify two distinct regimes, a cyclonic and anticyclonic regime, and examine the atmospheric and oceanic forcing that drives transitions between them. To assess the physical consistency and reliability of the reanalysis, we compare these circulation patterns against two independent observational lines of evidence: (1) trajectories from drifting icebergs and an Argo profiling float, and (2) multi-year records of along-strait velocity and heat transport from the Davis Strait mooring array, which provide an independent, in situ measure of the broader along-shelf flow south of the bay.

2 Data and methods

2.1 Data

2.1.1 Ocean reanalysis velocity data

The Global Ocean Physics Reanalysis (GLORYS12) reanalysis product, available from the Copernicus Marine Environment Monitoring Service (CMEMS, 2026b), provides 3D fields of temperature, salinity, and velocity on a $1/12°$ horizontal resolution grid ($\sim$9 km$\times$ 3–4 km) with 50 vertical levels and is available for the 1993–2026 period. We obtain monthly mean fields of the u and v ocean velocity components from the surface to 450 m depth over the 64–71°N, 50–65°W domain (Fig. 1).

We also evaluated the Global Ocean Physics Analysis and Forecast (CMEMS, 2026c) and the Arctic Ocean Physics Reanalysis (CMEMS, 2026a) products. All three reanalyses produced similar EOF results; however, the former covers only 2020–2026, and the latter excludes the Sullorsuaq Strait, precluding an accurate representation of the full bay geometry. GLORYS12 was therefore selected as the primary data source because it spans the full 1993–2026 period, enabling direct comparison with the Davis Strait mooring record (Sect. 2.1.3). The GLORYS12 product has been shown to perform well in studies focusing on West Greenland (Huang et al., 2026).

2.1.2 Atmospheric reanalysis and sea-ice motion data

The fifth generation European Centre for Medium-Range Weather Forecasts (ECMWF) atmospheric reanalysis (ERA5; Hersbach et al. 2023) provides hourly 10-m wind components (u_{10}, v_{10}) and sea-ice concentration at 0.25° horizontal resolution.

https://doi.org/10.5194/egusphere-2026-5183
Preprint. Discussion started: 7 September 2026

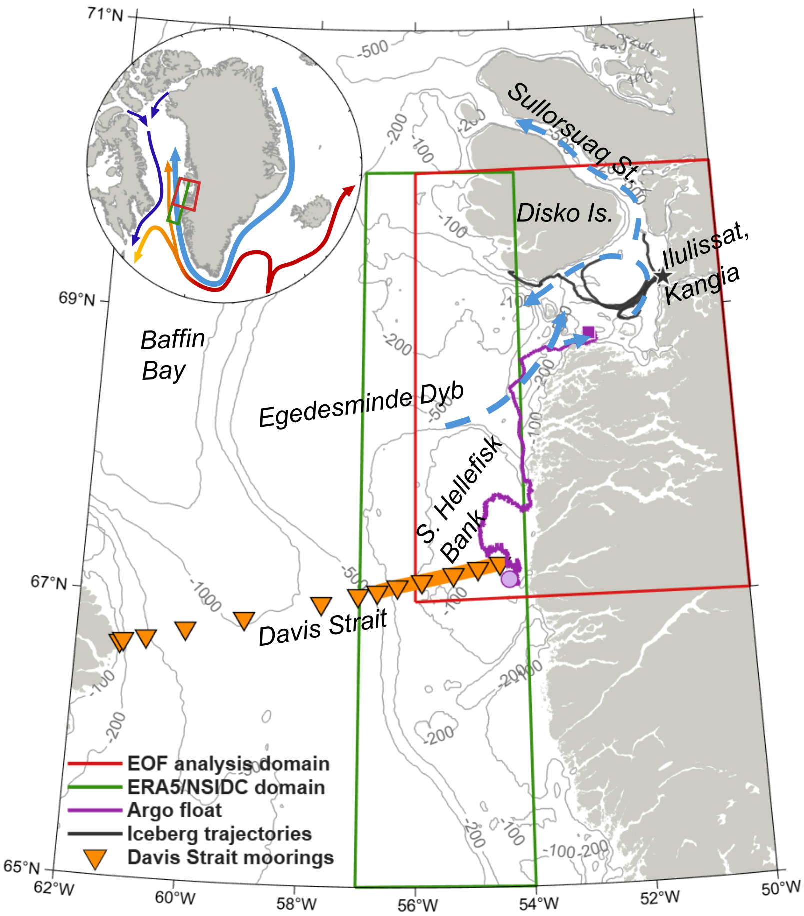

Figure 1. Study region and data domains in Qeqertarsuup Tunua (Disko Bay) and eastern Baffin Bay, with data domains indicated in the legend. An orange line connects the Davis Strait moorings within the coastal box (57–54.4°W) used for mean velocity and heat transport indices. Circle and square markers on the Argo float trajectory denote the first and last positions used in this study. The black star indicates the iceberg-beacon deployment at the mouth of the Kangia (Ilulissat Icefjord). Blue dashed arrows schematically represent surface circulation in Qeqertarsuup Tunua, adapted from Hansen et al. (2012). Grey contours show bathymetry from ETOPO1 (NOAA National Geophysical Data Center, 2009). The inset illustrates the large-scale circulation of Baffin Bay and the northern Labrador Sea, adapted from Huang et al. (2024): light blue for the East–West Greenland Current (WGC) carrying cool Polar-origin waters; red–orange for warm, saline Atlantic-origin water transported at depth with the WGC through Davis Strait; and dark blue for the Baffin Island Current (BIC).

Hourly data from the period 1993–2024 were obtained and averaged to daily means to match the temporal resolution of the sea-ice motion data.

https://doi.org/10.5194/egusphere-2026-5183
Preprint. Discussion started: 7 September 2026

The sea ice motion data were obtained from the National Snow and Ice Data Centre (Tschudi et al., 2019). Daily sea ice motion vectors covering 1993-2024 are available at a 25 km spatial resolution on the Equal-Area Scalable Earth (EASE) Grid. Vectors were rotated from the EASE grid to geographic (east–north) components and regridded to the ERA5 $0.25°$ grid.

2.1.3 Davis Strait mooring array observations

Estimates of ocean circulation from reanalysis are complemented with in-situ velocity measurements from the Davis Strait mooring array, approximately 350 km south of Qeqertarsuup Tunua (Fig. 1). As part of the Davis Strait Observing System, the Davis Strait mooring array comprises 15 stations, extending from the West Greenland shelf (54.5°W, 67.3°N) to the Baffin Island shelf (61.3°W, 66.7°N). In the following, we utilise daily, gridded sections of along-strait velocity (meridional velocities rotated by 77.3°), estimated using objective mapping and available for the 2004 to 2017 and 2020 to 2024 periods (Lenetsky, 2026). Details regarding mooring array configuration, data processing, gridding procedures, and uncertainty analysis can be found in Lenetsky (2026) and Lee (2024).

The gridded along-strait velocity is reduced to a single upper-layer, shelf-side index by averaging over a coastal box covering the West Greenland shelf side of the strait (57–54.4°W) and the upper 100 m (Fig.1). The daily box-averaged velocity is aggregated into monthly means, retaining a month only if at least 50% of its days have a valid box-averaged value, yielding $n = 206$ valid monthly values. This box-mean index is used in the analysis of Sect. 3.5(Fig.8). The cross-sectional composites presented in Sect. 3.5 (Fig.9) are instead formed from the full section: each grid cell is averaged over every month with valid data, without the 50% box-completeness restriction, so a larger set of $n = 243$ months contributes to the section fields.

Monthly estimates of the along-strait temperature transport (TT) in the same coastal box are computed as:

$$TT(t) = \rho c_p \int_{X_0}^{X_1}\int_{Z_0}^{Z_1} V_{(t,x,z)}(T_{(t,x,z)} - T_{\text{ref}})dz\,dx, \tag{1}$$

where $X_1 - X_0$ spans the West Greenland shelf (57–54.4°W), $Z_1 - Z_0$ spans the upper 100 m, V and T are the along-strait velocity and potential temperature at each grid point, ρ is the time- and box-mean potential density (1026.6 kg m^{-3}), $c_p = 3900$ (J kg^{-1} K^{-1}) is the specific heat capacity of seawater, and $T_{\text{ref}} = 0$°C is the reference temperature. Since the chosen coastal surface box does not bound a closed volume, and net transport is not balanced, the calculation depends on the choice of reference temperature (Schauer and Beszczynska-Möller, 2009). Following Johns et al. (2011), we refer to the calculated quantity as a temperature transport relative to 0°C rather than heat transport, with $T_{\text{ref}} = 0$°C chosen for consistency with previous Davis Strait and West Greenland shelf estimates (Cuny et al., 2005; Curry et al., 2011; Myers et al., 2021). The same 50% box-completeness criterion applied to the box-mean velocity above is applied to TT. To separate the contributions of the velocity and the temperature to TT, they are decomposed into their record means and monthly anomalies as $V_{(t,x,z)} = \bar{V}_{(x,z)} + V'_{(t,x,z)}$ and $T_{(t,x,z)} = \bar{T}_{(x,z)} + T'_{(t,x,z)}$, yielding

$$TT(t) = TT_{\bar{V}\bar{T}} + TT_{\bar{V}T'}(t) + TT_{V'\bar{T}}(t) + TT_{V'T'}(t), \tag{2}$$

https://doi.org/10.5194/egusphere-2026-5183
Preprint. Discussion started: 7 September 2026

which are referred to as the mean, temperature, velocity, and cross terms, respectively.

2.1.4 Iceberg drift trajectories

We deployed 18 GPS-equipped beacons on icebergs calved from Sermeq Kujalleq and free-drifting in Qeqertarsuup Tunua. All deployments were made in the vicinity of Ilulissat in June 2025 (Fig. 1). Beacons transmitted GPS positions at approximately hourly intervals, and all data are archived at the International Arctic Buoy Programme with the corresponding iceberg ID (IAPB, 2025).

Position records underwent a three-stage quality-control procedure. Pre-deployment position fixes recorded at the beacon activation site on land were removed by a geographic filter. The vessel transit phase, during which beacons moved at vessel speed ($> 1\,\mathrm{m\,s^{-1}}$) prior to deployment, was identified and removed by detecting the last fix exceeding this speed threshold, corroborated against the recorded deployment time in the field. Remaining outliers were flagged when any consecutive displacement exceeded $1.5\,\mathrm{m\,s^{-1}}$. Iceberg I2 (ID: 4449899) was observed to be grounded during the initial portion of its record; fixes prior to 21 June were excluded from all analyses for this beacon.

Only beacons with a free-drift record of at least 3 days duration and at least 20 quality-controlled position fixes were retained for analysis. Seven of the 18 deployed beacons satisfied these criteria, with free-drift durations ranging from 4.3 to 23 days and net displacements of 6–114 km. Drift velocities were computed from consecutive positions as the bearing and magnitude of each displacement vector, then decomposed into eastward (u) and northward (v) components. Segments with a time gap exceeding 2 days were excluded from velocity calculations.

2.1.5 Argo Float trajectory

We analyse the trajectory and drift velocity of Argo float 4903361 (Argo, 2026), which profiled in the study region from June to October 2022 at a nominal parking depth of ∼90 dbar. The float completed 540 profiles over this period at a mean cycle interval of approximately 6 hours, yielding a travel distance of ∼202 km along the West Greenland shelf. Drift velocities were derived from successive GPS positions of the float surfacing. The two Argo floats that drifted in Qeqertarsuup Tunua during 2022-2024 (Latuta et al., 2025) had parking depths that were too deep to be relevant to this study's focus on upper-layer circulation.

2.2 Methods

2.2.1 Empirical Orthogonal Function

The dominant mode of circulation variability is characterised using an Empirical Orthogonal Function (EOF) analysis of the monthly GLORYS12 fields over the Qeqertarsuup Tunua domain (50–56°W, 67–70°N, Fig. 1). The analysis was performed on the velocity fields at each depth level over the full available record (1993–2026). The zonal and meridional velocity anomalies (time-mean removed at each grid point) are decomposed simultaneously to retain the coupled variability of the vector field (Kaihatu et al., 1998; Marmorino et al., 1999), with each grid point weighted by $\sqrt{\cos\phi}$ to account for the meridional variation

https://doi.org/10.5194/egusphere-2026-5183
Preprint. Discussion started: 7 September 2026

in grid-cell area. Each mode comprises a spatial pattern and a Principal Component (PC) time series $\mathrm{PC}_k(t)$; the leading mode is denoted PC1.

The leading six modes account for 80.5% of the total variance, with individual contributions of 55.8% (EOF1), 10.3% (EOF2), 6.7% (EOF3), 3.0% (EOF4), 2.6% (EOF5), and 2.2% (EOF6). EOF1 is separated from EOF2 by more than six times the sampling error (North et al., 1982), confirming that it is statistically well separated from the higher modes. This paper focuses on EOF1, leaving the higher modes for future work.

Two distinct classifications of PC1 are used throughout, and we explicitly distinguish between them. First, the sign of PC1 defines the circulation regime: months with $\mathrm{PC1} > 0$ are termed cyclonic and months with $\mathrm{PC1} < 0$ anticyclonic, describing the inner-bay circulation patterns (Sect. 3.1). Second, for compositing we retain only months in which the mode is strongly expressed: EOF1$+$ months are those with $\mathrm{PC1} \geq +1\sigma$ and EOF1$-$ months those with $\mathrm{PC1} \leq -1\sigma$, where $\sigma = 1.008$ is the standard deviation of the full PC1 record; the remaining months are termed neutral.

To quantify the vertical coherence of the mode, the EOF1 computed at each depth level and its spatial pattern were compared with the surface reference pattern ($z = 0.5$ m) using an uncentered vector pattern correlation:

$$r_{\mathrm{map}}(z) = \frac{\sum_j \left(u_j^{\mathrm{ref}}\, u_j^z + v_j^{\mathrm{ref}}\, v_j^z\right)}{\sqrt{\sum_j \left[(u_j^{\mathrm{ref}})^2 + (v_j^{\mathrm{ref}})^2\right]}\ \sqrt{\sum_j \left[(u_j^z)^2 + (v_j^z)^2\right]}} \tag{3}$$

where $(u^{\mathrm{ref}}, v^{\mathrm{ref}})$ and (u^z, v^z) are the reference and depth-z EOF1 patterns, and the sum runs over the grid points j at which both patterns are defined. Separately, the coherence in timing was assessed from the Pearson correlation between PC1 at each depth and the surface-reference PC1. The significance level of the correlation was tested using a two-tailed t-test and the autocorrelation-adjusted effective sample size N_{eff}.

2.2.2 Ocean surface stress

The ocean surface stress (τ) estimation combines the air-ocean stress ($\tau_{\mathrm{air-water}}$) and the ice-ocean stress ($\tau_{\mathrm{ice-water}}$), following Dotto et al. (2018) as follows:

$$\tau = \alpha\, \tau_{\mathrm{ice-water}} + (1-\alpha)\, \tau_{\mathrm{air-water}} \tag{4}$$

$$\tau_{\mathrm{ice-water}} = \rho_{\mathrm{w}}\, C_{\mathrm{iw}}\, |U_{\mathrm{ice}}|\, U_{\mathrm{ice}} \tag{5}$$

$$\tau_{\mathrm{air-water}} = \rho_{\mathrm{air}}\, C_d\, |U_{\mathrm{air}}|\, U_{\mathrm{air}} \tag{6}$$

https://doi.org/10.5194/egusphere-2026-5183
Preprint. Discussion started: 7 September 2026

where α is sea-ice concentration, $\rho_\mathrm{w} = 1027\,\mathrm{kg\,m^{-3}}$ is seawater density, $C_\mathrm{d} = 1.25 \times 10^{-3}$ and $C_\mathrm{iw} = 5.5 \times 10^{-3}$ are the air–water and ice–water drag coefficients respectively, $\boldsymbol{U}_\mathrm{air}$ is the 10-m wind velocity, and $\boldsymbol{U}_\mathrm{ice}$ is the sea-ice drift velocity regridded to the ERA5 grid. A geographic sign convention is used throughout: τ_x is positive eastward, i.e. onshore towards the West Greenland coast, and τ_y is positive northward. Because the coast lies to the east of the forcing box, southward along-shelf stress ($\tau_\mathrm{y} < 0$) is upwelling-favourable and northward stress ($\tau_\mathrm{y} > 0$) downwelling-favourable.

Ocean surface stress, together with 10 m wind components were computed over the full ERA5–NSIDC domain and subsequently averaged over a West Greenland shelf box (57–54°W, 65–70°N; green box in Fig. 1). This box is deliberately wider than the EOF analysis domain to encompass the forcing over the full shelf, where it is most likely to drive the along- and cross-shelf Ekman transport that would influence the bay's circulation, and to exclude the bay interior, where NSIDC sea-ice motion vectors are unavailable.

3 Results

3.1 Upper-layer circulation pattern (EOF1)

The climatological mean upper-ocean circulation (0–100 m depth mean, 1993–2026) over the study region shows a coherent northward flow along the West Greenland shelfbreak and near the coast. Both progressively weaken north of 67°N, while retaining weak positive velocities and a tendency for on-shelf flow following the bathymetry of Egedesminde Dyb into Qeqertarsuup Tunua (Fig. 2a). West of 57°W, flow is predominantly southward, associated with the Baffin Island Current (BIC).

The leading EOF mode (EOF1) of the monthly surface velocity field (z = 0.5 m) explains 55.8% of the total variance (Fig. 2b). Its spatial structure is characterised by intensified inflow into Qeqertarsuup Tunua from the south, with currents following the 100 m isobath and diverting eastward through Egedesminde Dyb trough. The pattern captures cyclonic circulation inside the bay, with flow strengthening along the southern and eastern coastal margins and continuing northward into the Sullorsuaq Strait, or westward along the southern coast of Disko Island.

During EOF1+ months (PC1 $\geq +1\sigma$; $n = 70$), the 0–100 m composite circulation over the Baffin Bay domain (Fig. 2c) shows a well-defined northward WGC/WGCC. Near-coast velocities are intensified by 0.1–0.2 m s^{-1} along the shelf to approximately 67°N, where shallow bathymetry over Store Hellefisk Bank (67–68°N, 53–55°W, Fig.1) causes the current to spread onto the shelf and join the intensified flow along the 100 m isobath, before being channelled eastward by the Egedesminde Dyb trough and into the bay. The southward flow of the BIC, which extends close to the West Greenland shelfbreak near 57°N in the climatological mean (Fig. 2a), weakens during EOF1+ months (Fig. 2c). Inside Qeqertarsuup Tunua, the cyclonic circulation and northward outflow via Sullorsuaq Strait intensify (Fig. 2d).

During EOF1− months (PC1 $\leq -1\sigma$; $n = 67$), the large-scale flow along the West Greenland shelf reverses, with upper-layer velocities directed predominantly southward across Baffin Bay (Fig. 2e). A residual northward flow persists along the West Greenland shelfbreak south of 66°N, but the shelf itself is dominated by southward anomalies. Circulation within Qeqertarsuup Tunua reverses to anticyclonic, with southward flow through the Sullorsuaq Strait and westward flow along the bay's southern coastal boundary (Fig. 2f).

https://doi.org/10.5194/egusphere-2026-5183
Preprint. Discussion started: 7 September 2026

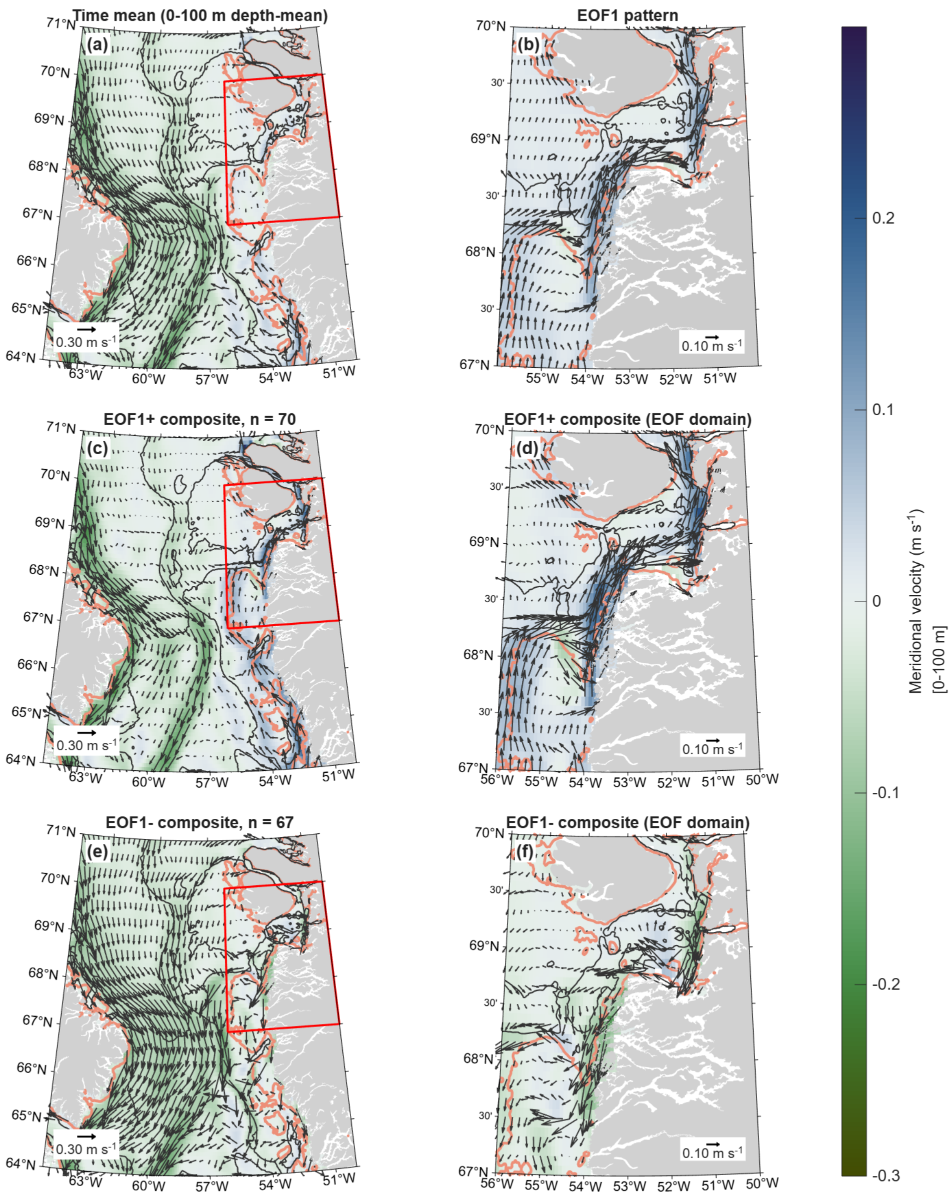

Figure 2. Composite circulation in Qeqertarsuup Tunua and Baffin Bay during cyclonic and anticyclonic regimes. Except for the EOF1 pattern in (b), all fields are the 0–100 m depth-mean velocity from GLORYS12, with shading showing the meridional (northward) component and black arrows the full velocity vector. Bathymetric contours are at -100 m (orange), -300 m and -1000 m (grey). (a) Time-mean circulation (1993–2026). (b) Scaled EOF1 pattern at $z = 0.5$ m (55.8% of variance), scaled by one standard deviation of PC1; its shading is an anomaly amplitude, shown on the shared colour scale for reference only. (c, e) Composite means for EOF1+ (PC1 $\geq +1\sigma$; $n = 70$) and EOF1$-$ (PC1 $\leq -1\sigma$; $n = 67$) months. (d, f) The same composites zoomed to the EOF analysis domain (red box in a, c, e).

https://doi.org/10.5194/egusphere-2026-5183
Preprint. Discussion started: 7 September 2026

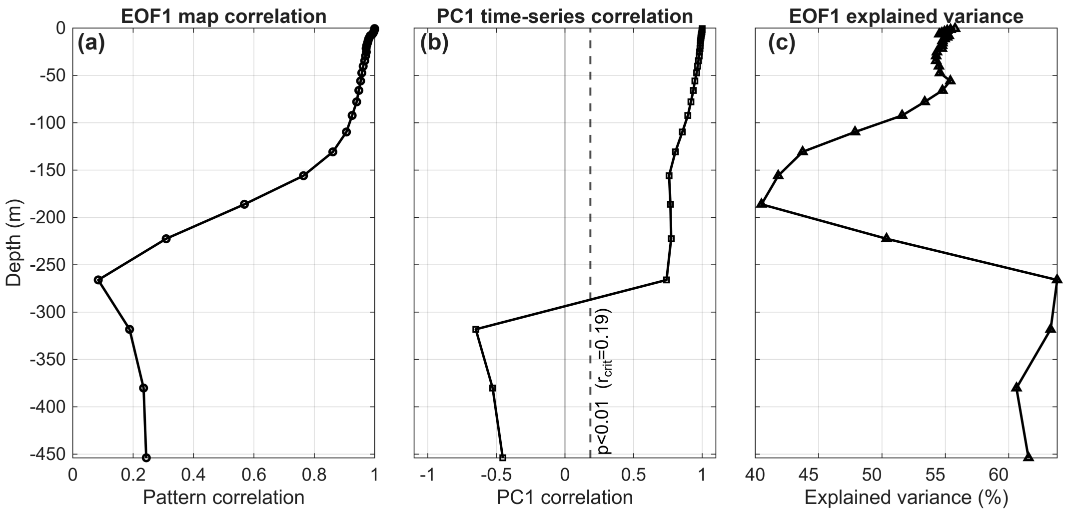

Figure 3. Vertical persistence of the leading EOF mode (EOF1) of upper-ocean circulation in Qeqertarsuup Tunua, computed from GLORYS12 monthly velocities (1993–2026). (a) Spatial pattern correlation between EOF1 at each depth and the reference pattern at z = 0.5 m. (b) Correlation between PC1 at each depth and the reference PC1 time series at z = 0.5 m. The dashed line marks the statistical significance threshold ($r_{crit} = 0.19$, p<0.01). (c) Explained variance of EOF1 at each depth.

3.1.1 Vertical coherence

The spatial pattern correlation between EOF1 computed at each depth and the surface reference (z = 0.5 m) remains above 0.80 throughout the upper ∼130 m, indicating that the same large-scale circulation structure is coherent through this layer (Fig. 3a). Below ∼130 m, the pattern correlation declines sharply, suggesting a structural reorganisation of the horizontal flow field rather than simple attenuation.

The PC1 time-series correlation (Fig. 3b) shows that the timing of the dominant mode remains highly correlated ($r > 0.90$) throughout the upper ∼100 m and remains statistically significant ($p < 0.01$) to approximately 270 m. This indicates that while the spatial structure of the circulation changes substantially below ∼130 m, the same forcing signal modulates the deeper flow on similar timescales and down to considerably greater depths. The explained variance (Fig. 3c) peaks near the surface at ∼56% and decreases monotonically to ∼42% at 200 m, confirming that EOF1 becomes progressively less dominant with depth as other dynamical processes contribute more to the variance.

3.1.2 Seasonality

The PC1 time series exhibits pronounced month-to-month variability throughout the 1993–2026 record, with a 12-month running mean revealing interannual variability superimposed on the dominant seasonal signal (Fig. 4a). The mean seasonal cycle accounts for 49.5% of the total PC1 variance: values are consistently negative from January through May, reach a minimum in March, rise sharply through summer to peak in August, and return towards zero in November–December (Fig. 4b).

https://doi.org/10.5194/egusphere-2026-5183
Preprint. Discussion started: 7 September 2026

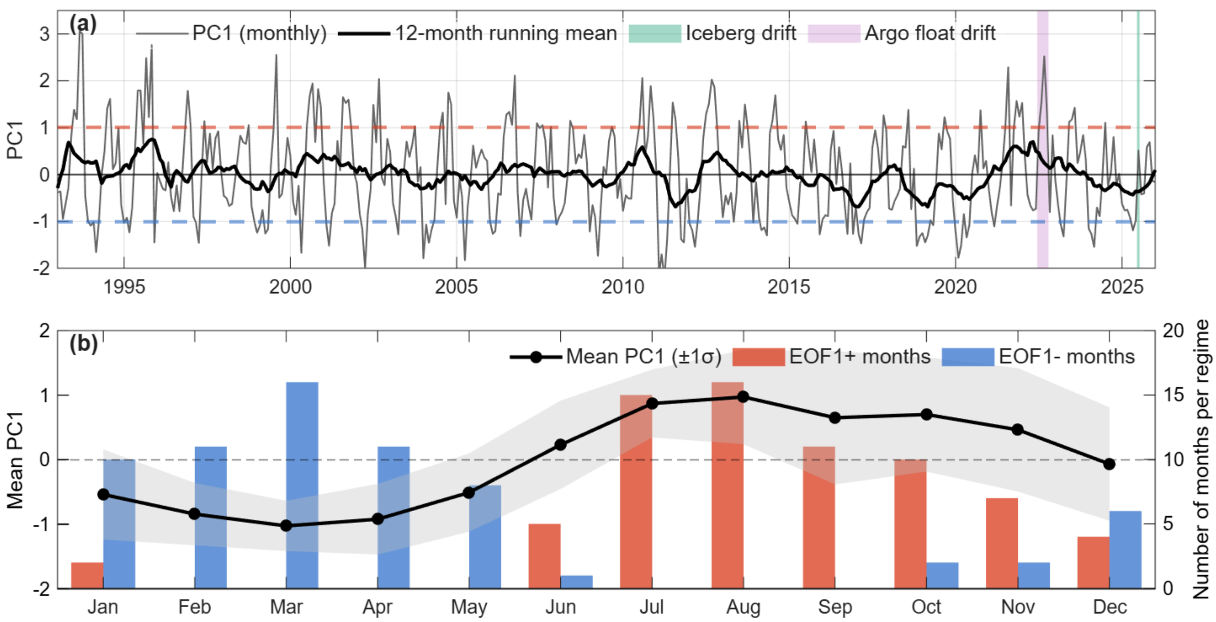

Figure 4. PC1 time series and seasonal characteristics of the dominant circulation mode in Qeqertarsuup Tunua for the full GLORYS12 record (1993–2026). (a) Monthly PC1 time series and 12-month running mean with the dashed lines indicating $\pm 1\sigma$ thresholds defining the EOF1+/EOF1− composite months. Drift periods of the icebergs and Argo float are shaded for reference. (b) Mean seasonal cycle of PC1 (left axis), with $\pm 1\sigma$ spread in grey shading, and the number of months classified as EOF1+ ($n = 70$) or EOF1− ($n = 67$) (right axis).

This seasonal evolution directly reflects the alternation between the two circulation regimes. Months below the -1σ threshold (EOF1−) occur predominantly between January and May and almost never in summer, while months above $+1\sigma$ (EOF1+) cluster in July–September and most frequently in August. The transitional months of June and November–December show the fewest exceedances of either sign.

The mean seasonal cycle crosses zero between the November and December monthly means, marking the climatological onset of the anticyclonic regime (Fig. 4b), but individual years transition over a wide window. Zero crossings of the 3-month running mean of PC1 place the onset of the cyclonic regime between May and June ($n = 31$ of 33 years) and its termination between November and December ($n = 28$), giving a cyclonic season of $\sim$6 months. These means exclude the years in which no crossing falls within the search window: 1996 and 2025 have no anticyclonic-to-cyclonic crossing between March and August, and 1996, 2000, 2002, 2016 and 2021 have no cyclonic-to-anticyclonic crossing between September and January. Neither the crossing date nor the season duration shows a significant trend.

Interannual variability in PC1 is small relative to the seasonal signal. The annual means range from -0.59 (2011) to $+0.52$ (2010), with a standard deviation ~ 3 times smaller than that of the full monthly record. Neither the annual nor the seasonal means show a significant trend, and the deseasoned PC1 anomaly decorrelates within one month, so successive annual means are effectively independent. The remainder of this study thus focuses on the seasonal alteration between the circulation regimes.

3.2 Atmospheric forcing

Over the 1993–2024 period for which the ERA5/NSIDC forcing and PC1 overlap, meridional wind (v_{10}) and ocean surface stress (τ_y) both correlate positively with PC1 at $r = 0.75$ ($p < 0.001$) in the raw monthly time series, and remain significant after removing the seasonal cycle ($r = 0.70$ and 0.67, respectively, both $p < 0.001$; Table 1). The zonal components correlate negatively and at comparable magnitude. Lag-correlation analysis of the deseasoned anomaly time series confirms that atmospheric forcing occurs simultaneously with the circulation state. None of the four atmospheric forcing variables show significant (at $p < 0.001$) correlation at positive lags beyond one month, i.e. forcing does not lead PC1 by more than one month, nor is there significant correlation at any negative lag.

The seasonal cycles of τ_y and τ_x closely follow that of PC1 (Fig. 5a). The stress is directed south–southeastward and is strongest in winter–spring, when $\mathrm{PC1} < 0$. It weakens through spring to near-zero magnitude in June, turns weakly northwestward in July–August as PC1 reaches its annual peak, and returns to southward through autumn as PC1 decreases towards zero, before intensifying towards the wintertime south-southeastward direction.

The composite means follow this seasonal structure (Table 1). The atmospheric composites comprise $n = 64$ EOF1− months, rather than the 67 of the full-record (1993–2026) circulation composites (Fig. 2), because of the shorter forcing record; the EOF1+ count ($n = 70$) is unchanged. EOF1+ months coincide with the period of weakest and most northwestward stress ($\bar{\tau}_\mathrm{y} = +0.008\,\mathrm{N\,m^{-2}}$, $\bar{\tau}_\mathrm{x} = -0.007\,\mathrm{N\,m^{-2}}$, $\bar{v}_{10} = +0.35\,\mathrm{m\,s^{-1}}$), whereas EOF1− months coincide with peak southward stress ($\bar{\tau}_\mathrm{y} = -0.074\,\mathrm{N\,m^{-2}}$, $\bar{v}_{10} = -4.46\,\mathrm{m\,s^{-1}}$), roughly nine times larger in magnitude than during EOF1+.

The spatial structure of the composite stress fields is shown in Fig. 5b,c. During EOF1+ months, the stress magnitude over the West Greenland shelf is weak throughout the domain with no spatially coherent direction north of 67° N. During EOF1− months, a strong, spatially coherent and intensified stress field covers the entire domain with vectors directed predominantly south-southeastward, aligning with the coast of Greenland.

3.3 Iceberg trajectories

Seven icebergs drifted freely in Qeqertarsuup Tunua between mid-June and mid-July 2025. Their freeboards were estimated from drone footage and ranged from 13–42 m, yielding drafts of approximately 91–294 m following the 1:7 freeboard-to-draft ratio as an approximation (Cenedese and Straneo, 2023). Their drift spanned a period during which the monthly PC1 transitioned from the anticyclonic regime in June (PC1 $= -0.98$) to the cyclonic regime in July (PC1 $= +0.51$; Fig. 6b). Both months are hence neutral by the $\pm 1\sigma$ composite criterion (Fig. 4a). This transition from negative to positive PC1 values, while modest in amplitude, provides an opportunity to compare observed drift with the two contrasting circulation regimes identified by the EOF analysis.

The five icebergs whose free-drift records were confined to June (I1, I3-6) drifted predominantly southwestward from their deployment site near Ilulissat (Fig. 6a). This anticyclonic trajectory is consistent with the June 2025 monthly mean circulation field (Fig. 6c), in which surface flow in the inner bay is directed southward and westward. Median drift speeds for these icebergs ranged from 0.05 to 0.14 $\mathrm{m\,s^{-1}}$, broadly comparable to the GLORYS12 surface velocity magnitudes in June.

https://doi.org/10.5194/egusphere-2026-5183
Preprint. Discussion started: 7 September 2026

Table 1. Correlations of PC1 with box-averaged atmospheric forcing variables (57–54° W, 65–70° N) and composite mean values during EOF1+ ($n = 70$) and EOF1− ($n = 64$) months, defined by $\mathrm{PC1} \geq +1\sigma$ and $\mathrm{PC1} \leq -1\sigma$ respectively, over the 1993–2024 period for which forcing and PC1 overlap. Significance is assessed with a two-tailed t-test on the autocorrelation-adjusted effective sample size N_{eff}; all correlations and all composite differences (Welch two-sample t-test) are significant at $p < 0.001$.

	Variable	r_{raw}	$N_{\mathrm{eff,raw}}$	r_{deseas}	$N_{\mathrm{eff,deseas}}$	EOF1+ composite	EOF1− composite	Units
Meridional								
v_{10}	10 m wind	+0.75	264	+0.70	371	+0.35	−4.46	$\mathrm{m\,s^{-1}}$
τ_y	Surface stress	+0.75	253	+0.67	379	+0.008	−0.074	$\mathrm{N\,m^{-2}}$
Zonal								
u_{10}	10 m wind	−0.72	275	−0.63	372	−0.49	+1.14	$\mathrm{m\,s^{-1}}$
τ_x	Surface stress	−0.67	318	−0.64	391	−0.007	+0.012	$\mathrm{N\,m^{-2}}$

One of the longest-lived icebergs, I7 (19.7 days, 114 km net displacement), drifted westward across the full breadth of the bay, also consistent with the predominantly anticyclonic June circulation. Its trajectory extended into July as PC1 shifted into the cyclonic regime, at which point the westward drift slowed and the track curved to the northwest, qualitatively consistent with the strengthening cyclonic component in the July composite (Fig. 6d).

Iceberg I2 was initially grounded and attained free drift on 21 June. After refloating, it drifted northward along the eastern flank of the bay over a 22.6-day period, reaching a net displacement of 36 km. This northward trajectory is anomalous relative to the predominantly anticyclonic southwestward motion of the June iceberg cohort and is consistent with a transition toward the cyclonic regime, which was established in July (Fig. 6d). The drift direction of I2 thus reflects the sub-monthly onset of the cyclonic regime within a month in which the monthly mean PC1 remains anticyclonic.

Overall, the iceberg trajectories corroborate the EOF1 framework at the surface. Iceberg drift is affected not only by surface currents, but also by wind forcing, iceberg shape, and tides, all of which influence motion (Cenedese and Straneo, 2023). Further, we note that iceberg drift integrates the near-surface circulation over the iceberg keel depth, which varied substantially among individual icebergs, and that the monthly GLORYS12 composites smooth out sub-monthly variability that is evident in the observed trajectories. With that caveat in mind, anticyclonic, southward-to-westward motion dominates during the anticyclonic month of June, while the onset of cyclonic, northward motion of iceberg I2 and the late-July curvature of iceberg I7 are consistent with the transition to the cyclonic regime. These results should therefore be interpreted as qualitative rather than quantitative validation of the circulation regimes.

3.4 Argo Float drift

The trajectory of Argo float 4903361 progresses from 67.1°N on the outer West Greenland shelf to 68.9°N inside Qeqertarsuup Tunua (Fig. 7), with an overall northward progression and a mean drift speed of $\sim 0.09\,\mathrm{m\,s^{-1}}$. The trajectory crosses Store

https://doi.org/10.5194/egusphere-2026-5183
Preprint. Discussion started: 7 September 2026

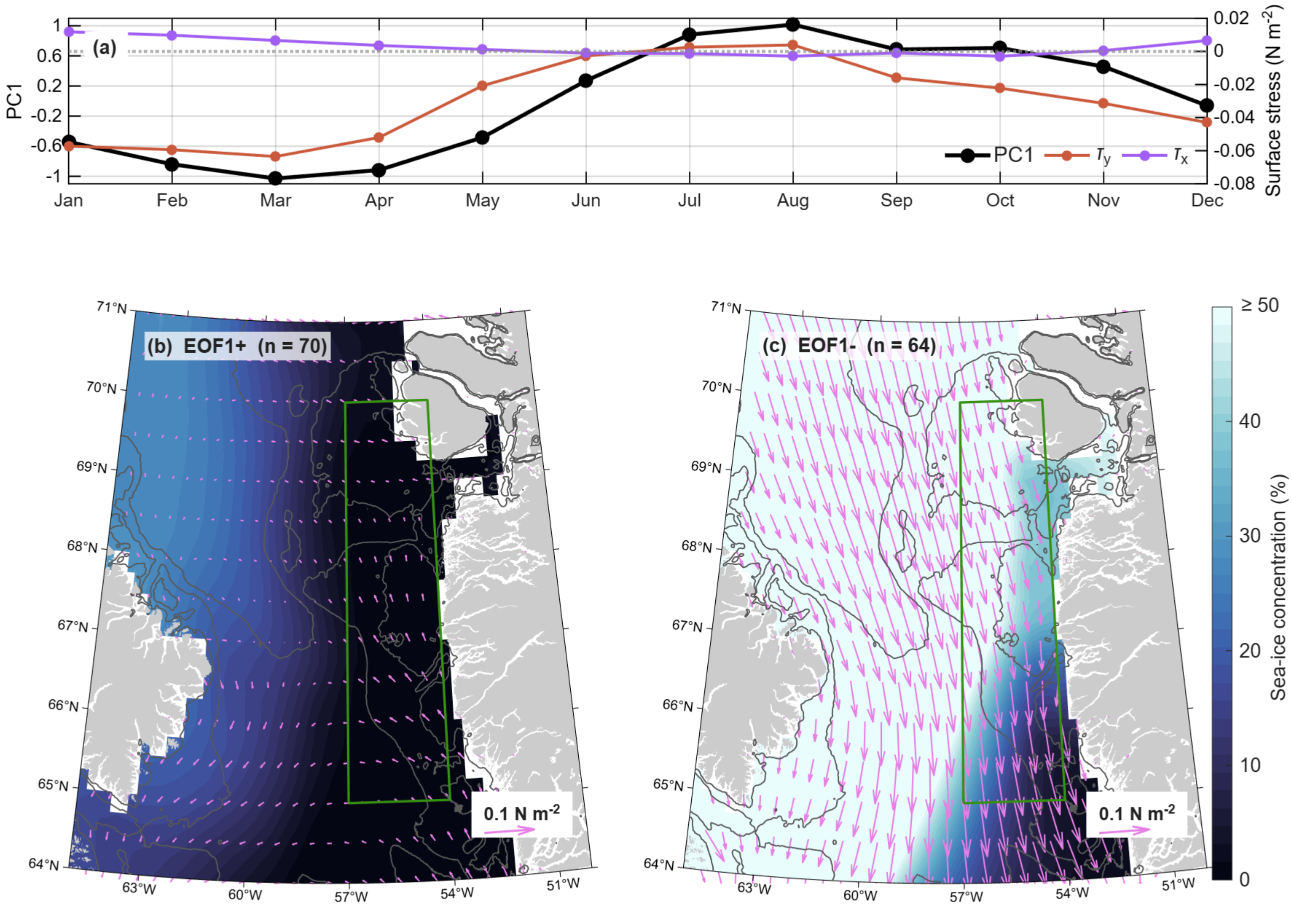

Figure 5. Seasonal cycles and EOF1 composites of atmospheric forcing. (a) Climatological seasonal cycle (monthly means) of PC1 (black; left y-axis) and ocean surface stress components (τ_x purple, τ_y orange; right y-axis) calculated over the green box (57–54° W, 65–70° N) in (b,c). (b,c) Composite-mean ocean surface stress vectors and sea-ice concentration as shading over months in the (b) EOF1+ (PC1 $\geq +1\sigma$; $n = 70$) and (c) EOF1− (PC1 $\leq -1\sigma$; $n = 64$) regimes.

Hellefisk Bank and follows Egedesminde Dyb into the bay (Fig. 7), with elevated drift speeds (0.25–0.30 $\mathrm{m\,s^{-1}}$) over the trough flanks, in line with topographic steering into the deep channel.

Daily-interpolated PC1 and float northward velocity are weakly correlated ($r = 0.29$, $N_{\mathrm{eff}} = 40$ after accounting for auto-correlation), but not significant at $\alpha = 0.05$ and are reported here as descriptive rather than as a hypothesis test. Of all the days, 89 fall in the EOF1+ months (PC1 $\geq +1\sigma$) and 31 in the neutral months, with mean drift speeds of 0.08 ± 0.04 and $0.07 \pm 0.05\,\mathrm{m\,s^{-1}}$ and mean northward velocities of 0.02 and 0.006 $\mathrm{m\,s^{-1}}$ respectively. The difference in mean northward velocity between the two states is small relative to the standard deviation of the individual displacements (0.12 $\mathrm{m\,s^{-1}}$) and we do not test it. No day in the record falls within an EOF1− month (PC1 $\leq -1\sigma$), so no direct comparison between the EOF1+ and EOF1− is therefore possible from this deployment. The deployment overlaps with an anomalously high PC1 peak relative

https://doi.org/10.5194/egusphere-2026-5183
Preprint. Discussion started: 7 September 2026

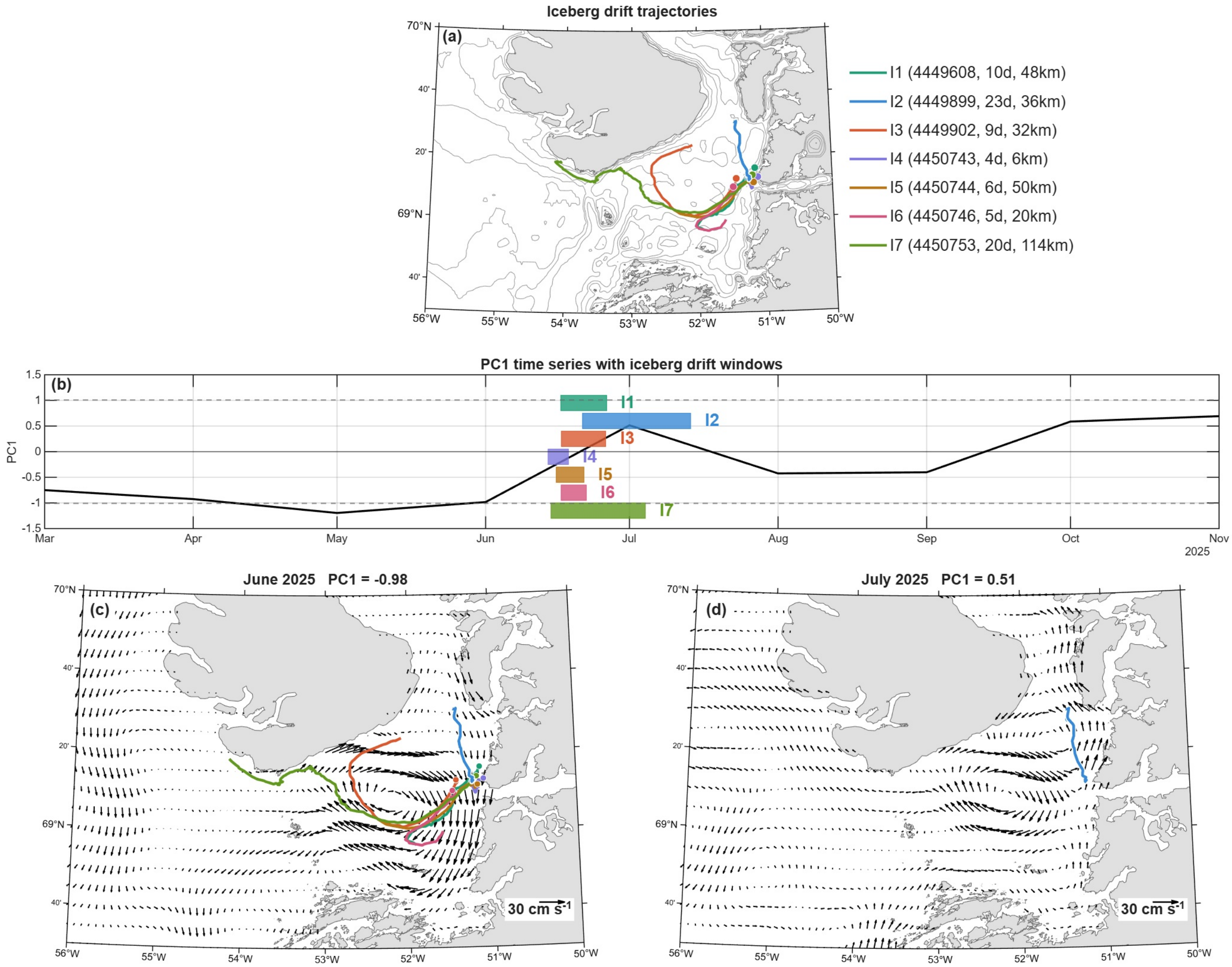

Figure 6. Iceberg drift trajectories in Qeqertarsuup Tunua during June–July 2025 and their relation to the dominant circulation mode. (a) Observed free-drift trajectories of the seven icebergs. Colours identify individual iceberg beacons as labelled, with the legend showing iceberg ID, total drift duration and net displacement. Filled circles mark the first fix of the free-drift phase. Bathymetric contours are drawn at -50, -100, -200, -300, and -500 m. (b) Monthly PC1 time series from the GLORYS12 EOF analysis for March–November 2025 (black) and the mean PC1 seasonal cycle (grey; full-record monthly climatology). Horizontal coloured bars indicate the free-drift period of each iceberg. Dashed lines mark $\pm 1\sigma$ of the full-record PC1 distribution. (c, d) Mean GLORYS12 surface velocity fields (black arrows) for June 2025 (PC1 $= -0.98$; anticyclonic) and July 2025 (PC1 $= +0.51$; cyclonic), respectively. Iceberg tracks active during each month are shown in colour.

to the full 1993–2026 record (Fig. 4a), further limiting the generalisability of this comparison, but the fastest segment of the trajectory was traversed in September 2022, with one of the highest PC1 values in the record ($+2.53$).

https://doi.org/10.5194/egusphere-2026-5183
Preprint. Discussion started: 7 September 2026

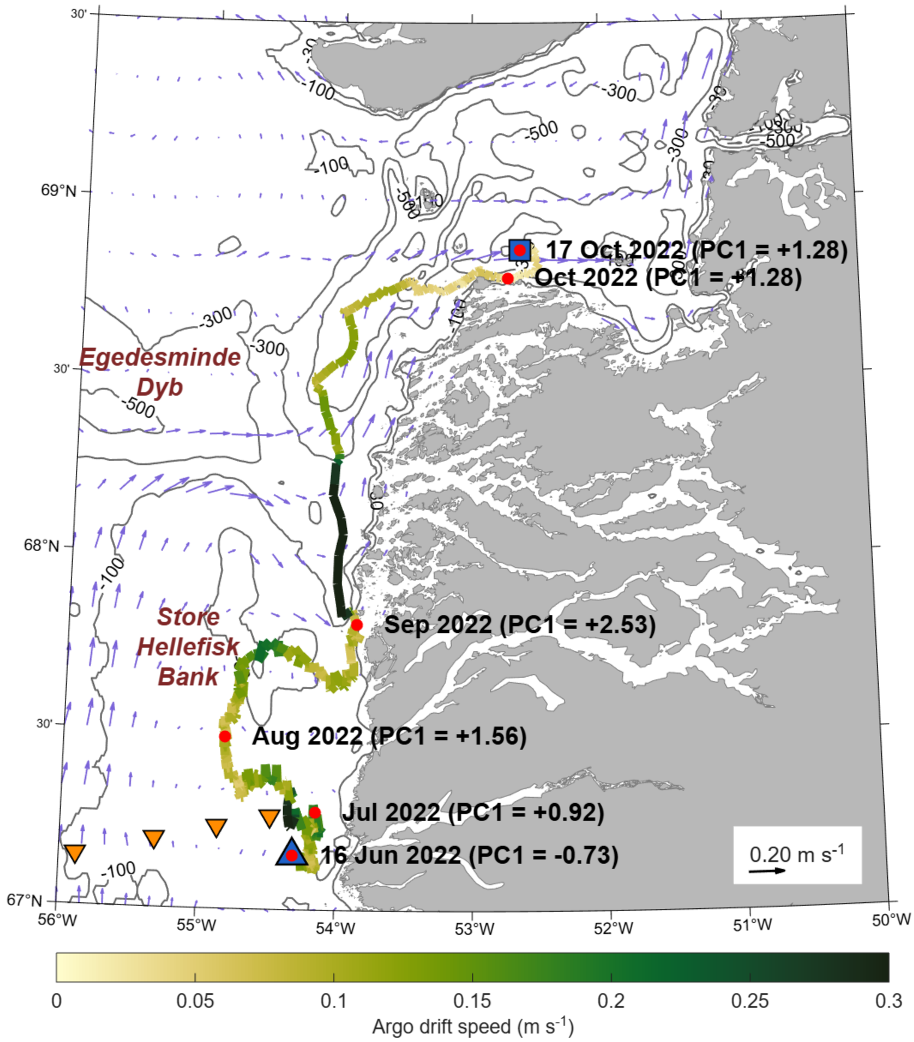

Figure 7. Trajectory of Argo float 4903361 from 16 June to 17 October 2022, coloured by daily mean drift speed (m s^{-1}). Purple arrows show the GLORYS12 monthly mean velocity for September 2022, depth-averaged over 0–100 m (every second grid-cell value is plotted). The blue triangle and square mark the first and last positions of the analysed record. Red dots mark the first profile of each month, annotated with the monthly PC1 value. Orange triangles indicate Davis Strait mooring locations. Grey lines are bathymetric contours (30, 100, 300, 500, 1000 m); coloured italic text marks the main bathymetric features.

3.5 Davis Strait velocity

305 To evaluate the connection between the Qeqertarsuup Tunua circulation mode and the large-scale flow along the West Greenland shelf, we compare PC1 with the along-strait velocity observations at Davis Strait (Fig. 8). We focus on the upper 100 m of the West Greenland shelf side of the strait (57–54.4°W, Fig.1), capturing the depth range most representative of the EOF1 pat-

https://doi.org/10.5194/egusphere-2026-5183
Preprint. Discussion started: 7 September 2026

tern (Fig. 3). Partitioned into EOF1+ and EOF1− months, the coastal box-mean index comprises $n = 42$ EOF1+ and $n = 35$ EOF1− months, whereas the section composites comprise $n = 45$ and $n = 46$ months (Fig. 9), respectively; the difference follows from the box-completeness criterion of Sect. 2.1.3.

The coastal box-averaged monthly mean velocity in this layer is predominantly northward, with a time-mean of $+0.03\,\mathrm{m\,s^{-1}}$ ($n = 206$ months; Fig. 8a). Southward flow occurs intermittently, most notably on the daily timescale, whereas monthly means become negative more rarely (12% of the time, most commonly in March). The velocity varies substantially at both seasonal and interannual timescales, with the largest negative monthly excursions concentrated during EOF1− months (Fig. 8a, blue shading).

The upper-layer velocity in the coastal box at Davis Strait correlates strongly with PC1 at zero lag ($r = +0.78$, $p < 0.001$; Fig. 8b). This is the strongest correlation across all tested lags and persists after removing the seasonal cycle from both time series ($r = +0.58$, $p < 0.001$; Fig. 8c). The raw monthly lag structure shows significant correlations at lags of ± 1 and $+2$ months, but these disappear entirely after deseasoning, indicating that they are an artefact of the seasonal cycle rather than evidence of a propagating signal with a distinct advective timescale (Appendix Table A1). The dominant structure is therefore one of quasi-simultaneous (shorter than 1 month) response, consistent with the atmospheric forcing results, where PC1 also peaks at zero lag with meridional ocean surface stress (Sect. 3.2).

The cross-sectional composites reveal the spatial structure underlying this correlation (Fig. 9). The time-mean section shows a concentrated northward-flowing core of $\sim 0.08\,\mathrm{m\,s^{-1}}$ centred on the West Greenland shelfbreak near 56.1–56.8°W, and to the west a predominantly southward surface-intensified flow (Fig. 9a). During EOF1+ months, the northward core along the Greenland shelf and shelfbreak is substantially enhanced across its entire depth range, with composite velocities reaching $+0.13\,\mathrm{m\,s^{-1}}$ (Fig. 9b; $n = 45$). The box-mean velocity over the shelf (0–100 m, 57–54.4°W) rises to $+0.06\,\mathrm{m\,s^{-1}}$ ($n = 42$), doubling from the $+0.03\,\mathrm{m\,s^{-1}}$ record mean.

During EOF1− months, the response is depth-dependent (Fig. 9c; $n = 46$): in the near-surface (0–50 m) layer the flow reverses to southward along the shelf, while below $\sim$100 m a weak northward signal is maintained and modulated in strength, with a core slightly shifting further west and deepening along the shelf slope. Averaged over the shelf box, the velocity drops to near zero ($+0.003\,\mathrm{m\,s^{-1}}$; $n = 35$). This contrast is confirmed by the anomaly composites (Fig. 9d–e): EOF1+ is associated with a positive velocity anomaly of up to $+0.06\,\mathrm{m\,s^{-1}}$ confined to the upper 100–150 m on the Greenland shelf, and extending to 400 m over the shelfbreak, while EOF1− exhibits a negative anomaly of comparable magnitude in the same region.

3.6 Temperature transport at Davis Strait

Temperature transport across the coastal box, referenced to 0°C, is $+3.43$ TW in the timeseries mean ($n = 205$ months) and varies seasonally by an order of magnitude from a climatological minimum of -0.18 TW in April to a maximum of $+9.21$ TW in September (Fig. 8d). Partitioned by EOF regimes, the temperature transport is $+7.56$ TW during EOF1+ months ($n = 39$) and $+0.66$ TW during EOF1− months ($n = 33$). It correlates with PC1 at $r = +0.71$ ($p < 0.001$), reducing to $r = +0.45$ for the deseasoned time series.

https://doi.org/10.5194/egusphere-2026-5183
Preprint. Discussion started: 7 September 2026

The decomposition separates this variability into contributions from the time-mean flow and monthly anomalies (Fig. 8d). The mean term is constant at $+1.85$ TW. As expected, the temperature and velocity terms average near zero over the full record, but exhibit a pronounced seasonal cycle with opposing directions. The temperature term ranges from $+3.4$ TW in August to -2.5 TW in April, and the velocity term from $+1.5$ TW in October to -2.0 TW in March. The two terms are in phase: both are positive in summer and autumn, and negative in winter and spring. The cross term is positive in every calendar month and is uncorrelated with PC1. The EOF regime dependence is found in the temperature and velocity terms, which change sign between EOF regimes, with $+2.1$ and $+1.4$ TW during EOF1+ to -1.7 and -1.6 TW during EOF1−. After removing the mean seasonal cycle from each series, the velocity term correlates with PC1 at $r = +0.60$ ($p < 0.001$), while the temperature term does not ($r = +0.22$, $p = 0.019$, not significant at $\alpha = 0.01$).

4 Discussion

4.1 A local expression of basin-scale Baffin Bay forcing

The seasonal alternation between cyclonic and anticyclonic circulation in Qeqertarsuup Tunua represents the local expression of a seasonal signal that extends across Baffin Bay. Using a high-resolution coupled ice–ocean model, Shan et al. (2024) demonstrated that the leading EOF of the Baffin Bay barotropic streamfunction exhibits a seasonal cycle directly comparable to PC1 identified in this study: a positive surface stress curl anomaly along the 1000 m isobath intensifies the cyclonic gyre in summer–autumn, while a negative anomaly weakens it in winter–spring. On the West Greenland shelf, where our forcing box lies, this basin-scale seasonality is expressed locally as a reversal of the along-shelf ocean surface stress, shifting from strongly southward in winter to weakly northward in July–August (Sect. 3.2). The cross-shelf Ekman transport implied by this stress reversal transitions from offshore during EOF1− to weakly onshore during EOF1+. As the along-coast winds regulate the strength of coastal current through the cross-shelf sea-surface-height gradient (Pacini et al., 2020; Foukal and Pickart, 2023), the upwelling-favourable conditions of EOF1− composite would lower coastal sea-surface height and thus weaken the northward shelf flow, consistent with the reversal of the near-surface ($\sim$100 m) flow along the West Greenland shelf at Davis Strait and the negative velocity anomalies extending to $\sim$400 m over the shelf and slope (Fig. 9c,e).

This wind-driven reversal is in agreement with the broader West Greenland boundary current system. Gou et al. (2022) show that the forcing of the WGC and WGCC transitions along the shelf: buoyancy forcing dominates south of 64°N, while wind forcing becomes increasingly important towards Davis Strait, where upwelling-favourable winds prevail in all seasons except summer and exert a stronger control than the downwelling-favourable summer winds. They further find that the WGCC is predominantly buoyancy-driven, except in winter. During this season, strong upwelling-favourable winds render it primarily wind-driven (Gou et al., 2022), which is the season corresponding to our anticyclonic regime. Direct observational comparisons of wind forcing and boundary-current response are limited to the southwest Greenland shelf near Cape Farewell, where Pacini and Pickart (2023) show that during the forward tip jet events the upwelling-favourable winds weaken the shelfbreak flow, but only on synoptic rather than seasonal timescales. Additionally, remote wind forcing over the East Greenland shelf regulates the volume transport and the position of the WGCC, the latter migrating laterally along the shelf in a chaotic manner (Pacini

https://doi.org/10.5194/egusphere-2026-5183
Preprint. Discussion started: 7 September 2026

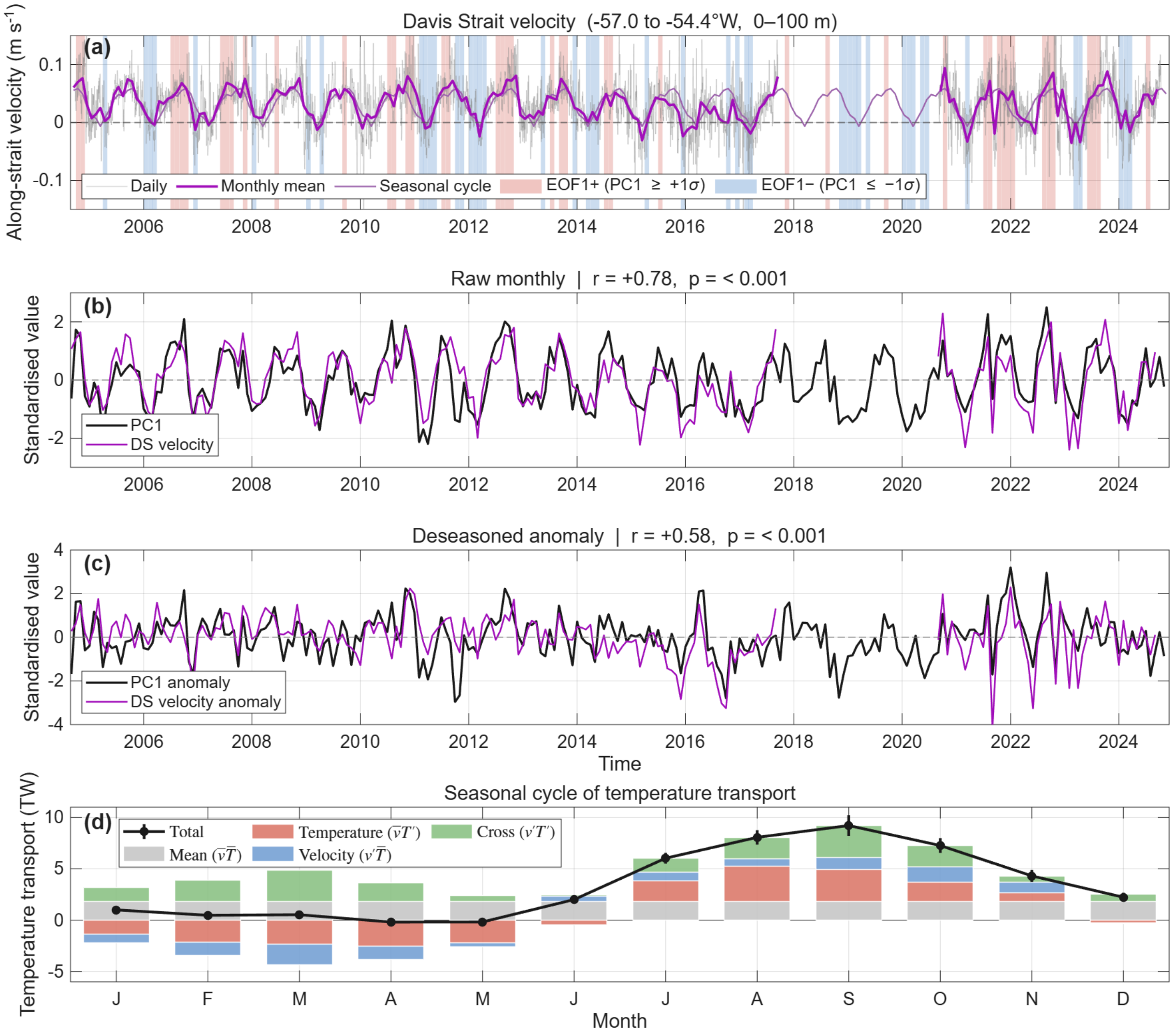

Figure 8. (a) Along-strait velocity in the upper layer (0–100 m) of the Davis Strait, within the coastal box along the West Greenland shelf (57–54.4°W), from the Davis Strait mooring array. Daily (grey) and monthly (thick purple) mean values are shown for the full 2004–2024 record, with a data gap in 2017–2020, with a mean seasonal cycle (thin purple) in the background. Positive values denote flow into Baffin Bay. Background shading indicates months when PC1 exceeds $+1\sigma$ (red; EOF1+ months) or falls below -1σ (blue; EOF1- months). (b–c) Standardised time series of PC1 (black) and monthly mean Davis Strait velocity (purple) for raw monthly values in (b) and after removing the monthly climatology from both series in (c). Correlation coefficients are indicated in each panel. (d) Monthly climatology of the ocean temperature transport across the same box, referenced to 0°C. Bars show the four terms of the Reynolds decomposition, stacked around zero, with negative contributions oriented downward. The colour of each bar corresponds to the terms outlined in the legend. The black line is their sum, the total temperature transport, with vertical bars showing the standard error of the monthly mean.

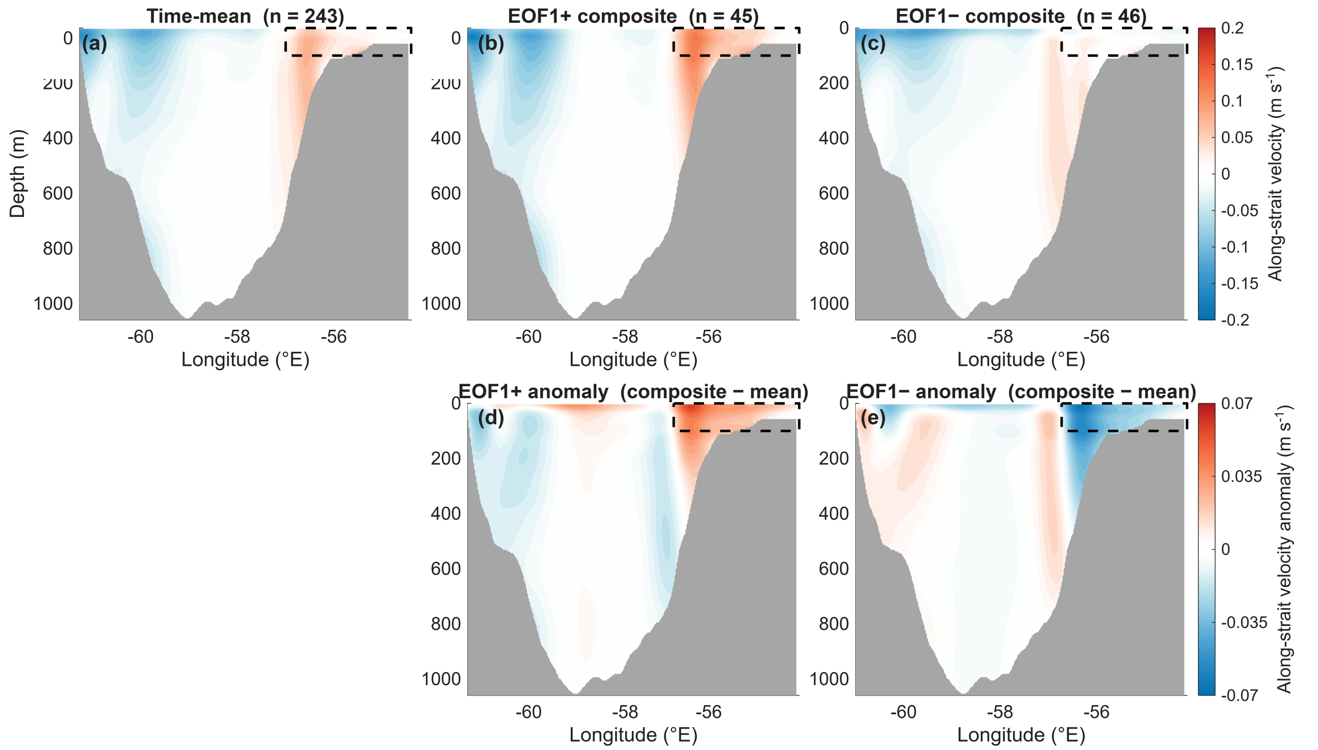

Figure 9. Davis Strait along-strait velocity cross-sections. (a) Time-mean velocity (n = 243 months). (b) Composite mean during EOF1+ months (PC1 $\geq +1\sigma$; n = 45). (c) Composite mean during EOF1- months (PC1 $\leq -1\sigma$; n = 46). Panels (a–c) share a common colour scale. (d) EOF1+ velocity anomaly (composite minus time-mean). (e) EOF1- velocity anomaly (composite minus time-mean). Panels (d–e) share a common anomaly colour scale. Grey shading indicates the seafloor. The dashed box outlines the longitude and depth range used for the box-mean analysis. Positive velocity indicates flow into Baffin Bay.

et al., 2020; Foukal and Pickart, 2023), whereas such a mechanism has not yet been observed further north along the West Greenland Shelf. In contrast, the EOF1 response in Qeqertarsuup Tunua is local and near-instantaneous (Sect. 3.2), resulting in a more distinct seasonal cycle than that observed near Cape Farewell (Foukal and Pickart, 2023). To our knowledge, the influence of local winds has not been examined at or north of Davis Strait, and the drivers of West Greenland Shelf Water and West Greenland Irminger Water transport variability through the strait remain uncertain (Lenetsky, 2026).

The fact that PC1 shows a strong zero-lag correlation with the upper-layer velocity in the Davis Strait confirms that the bay's circulation mode is coherent with the large-scale along-shelf flow. This finding is consistent with historical current-meter data showing that Baffin Bay circulation is stronger at all depths in summer–autumn than in winter–spring (Tang et al., 2004). Similarly, Huang et al. (2024) find that a positive wind-stress-curl anomaly over Baffin Bay in July–October enhances the cyclonic circulation and eastward recirculation of the western boundary current in the southern part of the bay. Consistent with this timing, Curry et al. (2014) and Lenetsky (2026) show that the northward transport of West Greenland Shelf Water, and that of the underlying West Greenland Irminger Water, peaks in September–November and is weakest in February–April. The most

https://doi.org/10.5194/egusphere-2026-5183
Preprint. Discussion started: 7 September 2026

notable expression of this coherence occurs in 2010–2011. In December 2010 the net volume transport at Davis Strait reversed from southward to northward, and the modelled heat transport into Qeqertarsuup Tunua during the winter 2010–2011 exceeded all other winters by more than 1.1 TW (Myers et al., 2021). PC1 similarly identifies 2010 as the year with the most persistent cyclonic regime in the record, having both the latest termination of the cyclonic regime and the longest cyclonic season (8.2 months), thus maintaining the heat-advection pathway into Qeqertarsuup Tunua well into wintertime.

4.2 Implications for heat transport and deep water renewal in Qeqertarsuup Tunua

EOF1 represents an upper-ocean mode that is coherent down to $\sim$130 m depth and does not directly control the delivery of warm West Greenland Irminger Water at depth to the bay's interior. Deep renewal is instead controlled by the $\sim$300 m Egedesminde Dyb Sill and by density-driven processes (Gladish et al., 2015a, b; Latuta et al., 2025), which likely operate independently of the upper-layer circulation regime. Nevertheless, EOF1 remains relevant to the bay's heat budget through its influence on the advection of West Greenland Shelf Water, the upper-layer component of the WGC. The temperature transport across the West Greenland shelf at Davis Strait is an order of magnitude larger during the cyclonic regime compared to the anticyclonic regime ($+7.56$ against $+0.66$ TW; Sect. 3.6), and it is correlated with PC1 at $r = +0.71$ (Sect. 3.6).

Two seasonal cycles combine to produce this contrast. Observations from a mooring in the Davis Strait show that West Greenland Shelf Water velocity along the West Greenland shelf peaks in autumn and is weakest in spring, while its temperature reaches a maximum in August ($\bar{T} = 4.2$°C) and a minimum in March ($\bar{T} = -1.0$°C) (Curry et al., 2014; Lenetsky, 2026), so that warm water and strong northward flow coincide during EOF1$+$, and cold water and weak or reversed flow during EOF1$-$ (Sect. 3.6). Such reinforcement is a seasonal-cycle effect; however, once the seasonal cycle is removed, only the velocity term remains correlated with PC1, while the temperature term does not. Therefore, the temperature-transport variability associated with the circulation mode is driven by the strength and direction of the shelf flow rather than by West Greenland Shelf Water temperature. The cross term adds a further $+1.6$ TW to the record mean, but unlike the temperature and velocity terms, does not distinguish the two circulation regimes.

Although EOF1 and deep renewal are dynamically distinct, their seasonal cycles are nearly out of phase, and we suggest that they share a driver: the upwelling-favourable conditions of the EOF1$-$ composite. Latuta et al. (2025) observe West Greenland Irminger Water renewal each spring, when densification along the West Greenland shelf lifts isopycnals above sill depth (Gladish et al., 2015a, b), and an additional episodic renewal in November–December 2022 driven by strong, persistent upwelling-favourable winds over the sill. Both fall in months when PC1 is at, or approaching, its seasonal minimum: November 2022 is that year's PC1 minimum (-0.80), and the PC1 minima of April 2023 (-1.32) and March 2024 (-1.55) fall within the observed spring renewal windows. We interpret the correspondence as a common forcing rather than a causal chain, since the same wind reversal which establishes the anticyclonic upper-layer regime may also drive the offshore Ekman transport that raises dense isopycnals towards the sill.

https://doi.org/10.5194/egusphere-2026-5183
Preprint. Discussion started: 7 September 2026

4.3 Implications for marine ecology

Qeqertarsuup Tunua is one of the most productive regions in Greenland and supports major fisheries (Andersen, 1981; Møller et al., 2023). The seasonally reversing circulation shapes the physical environment that determines the productivity by affecting the distribution of nutrients, heat, and freshwater, as well as larval dispersal.

Nitrate availability in the surface waters of the bay is strongly seasonal: relatively high in the well-mixed winter water column, drawn down by the spring bloom to depletion through summer, and renewed in autumn by increased vertical mixing (Andersen, 1981; Møller et al., 2023). As such, after the spring phytoplankton bloom, productivity is limited by nitrate availability (Dünweber et al., 2010; Hansen et al., 2012). The most direct link between the circulation in the bay and productivity is the dispersal of nutrient-enriched, glacially modified water from Kangia. The subglacial discharge plume of Sermeq Kujalleq rises from the grounding line, entraining deeper, nutrient-rich water and transporting it to the photic zone (Beaird et al., 2017; Meire et al., 2017; Oliver et al., 2023; Wood et al., 2025). Wood et al. (2025) estimate that this process increases summer Chl-a in Sullorsuaq Strait by approximately threefold and enhances total primary productivity across the bay by up to $\sim$40%. Oliver et al. (2023) attribute a significant fraction of the interannual variability in satellite-derived Chl-a in northern Qeqertarsuup Tunua to this nitrate enrichment.

Glacially modified water exits Kangia as a buoyant current (Beaird et al., 2017) following two export pathways identified in both modelled and remotely sensed Chl-a fields: a main northward pathway through Sullorsuaq Strait and a secondary cyclonic route along the southern coast of Disko Island (Beaird et al., 2017; Wood et al., 2025). This double pathway corresponds to the cyclonic regime, in which surface waters circulate cyclonically around the bay and the majority of flow exits northwards through Sullorsuaq Strait. This circulation serves as the physical mechanism responsible for both the retention and the export of nutrient-enriched glacially modified water. It will nevertheless require further investigation, using coupled biogeochemical modelling or remote sensing products, to determine whether variability in the timing of the seasonal reversal results in detectable variability in bay-scale productivity.

The way in which circulation patterns operate has a direct influence on the dispersal of the larvae of the northern shrimp (*Pandalus borealis*). Northern shrimp represents Greenland's most important fishery, with its earliest fishing grounds historically located around Qeqertarsuup Tunua (Hamilton et al., 2003). Since 2010, the bay and the area of its trough (Northwest Atlantic Fisheries Organization (NAFO) areas 1A and 1B) have accounted for more than $\sim$80% of shrimp catches within West Greenland's Exclusive Economic Zone (NAFO areas 1A-1F) (Burmeister, 2025) and as much as 26% of the national shrimp catch (Krawczyk et al., 2024). Most fishing operations take place along the shallow borders of Egedesminde Dyb trough and near-shore areas within Qeqertarsuup Tunua (Burmeister, 2025). The species has a pelagic larval phase of approximately 85 days, from April to early October, during which near-surface currents govern dispersal and retention (Le Corre et al., 2020). Le Corre et al. (2020) state that the highest densities of shrimp larvae settle near Disko Island, with the WGC transporting larvae northward along the West Greenland shelf into the bay, where relatively weak currents favour retention over dispersal. Moreover, the greatest variability in current velocity during the larval period occurs at its beginning and end, around April and October, which correspond to the months of EOF1+/EOF1− transition (Fig. 4b). The timing of the seasonal reversal may

https://doi.org/10.5194/egusphere-2026-5183
Preprint. Discussion started: 7 September 2026

thus be a significant factor in interannual variability in the retention versus export of larvae, thereby enhancing or limiting connectivity among geographically separated populations. For example, a year with a later onset of an EOF1+ regime, or its shorter duration, might reduce the transport of larvae from farther south along the West Greenland Shelf into Qeqertarsuup Tunua, thus potentially reducing settlement success in the bay.

4.4 Reanalysis limitations

Reanalysis products, in this case GLORYS12 at $1/12°$ resolution, provide the only practical means of examining the full seasonal circulation cycle in Qeqertarsuup Tunua due to the lack of in situ current measurements within the bay. Nevertheless, several limitations need to be considered when interpreting these results.

First, GLORYS12 represents Greenland freshwater input as a climatological surface flux, without spatially explicit and interannually varying runoff from individual outlet glaciers (Jean-Michel et al., 2021). Additionally, the model does not represent the subglacial discharge plume of Sermeq Kujalleq, and Kangia as a whole remains unresolved at $1/12°$. Despite these limitations, the observed northward, near-coastal outflow from Kangia (Beaird et al., 2017) is consistent with the cyclonic regime's circulation pattern. The seasonal increase in freshwater forcing, which rises through spring to a July–August peak (Mernild et al., 2015; Enderlin et al., 2016; Kajanto et al., 2023; Wood et al., 2025; Picton et al., 2025), coincides with the onset and peak of the cyclonic regime. However, it remains unclear whether this freshwater input simply coincides with or actively reinforces the cyclonic pattern, as this cannot be resolved based on GLORYS12 alone.

Second, GLORYS12 does not adequately resolve the ~300 m Egedesminde Dyb Sill, which regulates dense-water exchange between the shelf and the bay interior (Gladish et al., 2015a). Exploratory deep-level EOF analyses indicate inflow originating from the north, rather than the West Greenland Irminger Water propagation from Davis Strait expected from observations (Gladish et al., 2015a). Consequently, the analysis is not extended to deep renewal processes, which are reserved for future research requiring independent in situ velocity and hydrographic validation that is currently unavailable.

Third, for the upper ~130 m, where EOF1 is coherent (Fig. 3), independent observations support the reliability of the reanalysis. Near Davis Strait, the strong correlation between PC1 and Davis Strait mooring along-strait velocity (Fig. 8) substantiates the realism of the upper-layer seasonal signal. Additionally, the seven iceberg tracks are qualitatively consistent with the corresponding monthly composites (Sect. 3.3). The Argo float offers a weaker constraint: although it drifted northward into the bay during a period dominated by EOF1+ months, the correlation between its northward velocity and PC1 is not significant. Therefore, the trajectory is consistent with the reanalysis rather than providing a test of it.

5 Conclusions

We provide the first quantitative characterisation of circulation variability in Qeqertarsuup Tunua (Disko Bay), West Greenland. The GLORYS12 reanalysis (monthly means, 1993–2026) was used to extract the dominant circulation mode within the bay, and the EOF analysis of the upper-ocean velocity field identifies a single dominant mode, EOF1, explaining 55.8% of the variance. EOF1 represents a seasonal reversal between a cyclonic and an anticyclonic regime. The cyclonic regime has a strengthened West Greenland Current feeding an intensified cyclonic circulation channelled into the bay through Egedesminde Dyb. In the anticyclonic regime, the inner-bay flow reverses to southward through Sullorsuaq Strait (Vaigat Strait) and becomes anticyclonic within the bay. This EOF1 mode is spatially coherent throughout the upper $\sim$130 m.

The seasonal cycle accounts for 49.5% of the variance of PC1, the principal component time series of EOF1. The cyclonic regime prevails from approximately May–June to November–December, peaking in August, while the anticyclonic regime dominates from January to April. This alternation is driven locally by the reversal of the along-shelf ocean surface stress. Meridional surface stress exhibits a strong correlation with PC1 at zero lag ($r = 0.75$ in the raw monthly series), with no significant lead, indicating a near-instantaneous local response rather than remote advection.

The EOF1 calculated within Qeqertarsuup Tunua is also consistent with the large-scale along-shelf flow in the Davis Strait. The observed Davis Strait upper-layer along-strait velocity correlates with PC1 at $r = +0.78$ at zero lag, and at $r = +0.58$ after removing the seasonal cycle. The mean along-strait velocity over the shelf approximately doubles during EOF1+ months relative to the record mean and decreases to near zero during EOF1− months.

Independent Lagrangian evidence from drifting icebergs and an Argo float is qualitatively consistent with the two circulation modes and the EOF1 composites. However, given its limited temporal coverage, these observations support rather than formally test the reanalysis-based results.

The timing and duration of the cyclonic season define the period over which the warmest and fastest-flowing shelf waters reach Qeqertarsuup Tunua before winter cooling. Temperature transport along the West Greenland shelf towards the bay is an order of magnitude larger during EOF1+ than during EOF1− months ($+7.56$ against $+0.66$ TW, $r = +0.71$ with PC1), a contrast dominated by the strength and direction of the shelf flow rather than by the temperature of the water. The seasonal alternation between the two circulation regimes therefore has implications not only for the bay's heat budget, but also for the near-surface transport of freshwater, nutrients, and larvae.

Data availability. ERA5 data are available at the Copernicus Climate Change Service (C3S) Climate Data Store (CDS) at https://doi.org/10.24381/cds.adbb2d47. Bathymetry data are available at https://doi.org/10.7289/V5C8276M. Argo float data are available at: https://fleetmonitoring.euro-argo.eu/float/4903361. GLORYS12 reanalysis product is available at https://doi.org/10.48670/moi-00021. Sea ice motion data are available at: https://nsidc.org/data/nsidc-0116/versions/4. Iceberg drift trajectories recorded during this study are available at: https://iabp.apl.uw.edu/DiskoBay_2025.html. Davis Strait mooring dataset is available at https://arcticdata.io/catalog/view/doi%3A10.18739%2FA2416T169.

https://doi.org/10.5194/egusphere-2026-5183
Preprint. Discussion started: 7 September 2026

Table A1. Lagged correlations between PC1 and Davis Strait upper-layer (0–100 m) along-strait velocity (57–54.4°W). Correlations are shown for raw monthly values and deseasoned anomalies. Significance is assessed using a t-test on the effective sample size N_{eff}, which adjusts the number of monthly values for the lag-1 autocorrelation of both series. Asterisks denote significance at $p < 0.01$. Positive lag = Davis Strait velocity leads PC1.

	Raw monthly			Deseasoned anomaly		
Lag (months)	r	N_{eff}	sig.	r	N_{eff}	sig.
−6	−0.50	94	***	+0.02	163	
−5	−0.51	95	***	−0.06	163	
−4	−0.39	95	***	−0.15	165	
−3	−0.12	95		−0.10	165	
−2	+0.21	98		−0.01	168	
−1	+0.51	97	***	+0.14	167	
0	**+0.78**	**98**	***	**+0.58**	**168**	***
+1	+0.53	98	***	+0.19	168	
+2	+0.28	98	***	+0.00	166	
+3	+0.03	96		−0.04	164	
+4	−0.26	95		−0.11	163	
+5	−0.44	95	***	−0.06	162	
+6	−0.52	94	***	−0.04	162	

Appendix A

Author contributions. LL: Writing – review and editing, Writing – original draft, Visualization, Methodology, Investigation, Formal analysis, Conceptualization. ED and LH: Conceptualization, Methodology, Visualization, Supervision, Writing - review and editing. JEL: Methodology, Data curation, Writing - review and editing

Competing interests. The authors declare that they have no conflict of interest.

Acknowledgements. We thank Cy Keener for processing the iceberg-geometry imagery and for providing the means to tag the icebergs used in this study. We thank John Davidsen for his expertise in safely and effectively carrying out the fieldwork as our captain, and Angela Barbara Muhmenthaler for assisting with the fieldwork. This work was supported financially by the Research Council of Norway through the project ClimateNarratives (no. 324520), the Meltzer Project Grant (no.32375) awarded to Linda Latuta, and the Fulbright Arctic Initiative grant awarded to Lars H. Smedsrud. Jed Lenetsky received funding from the National Science Foundation (awards OPP1902595 & OPP1902628).

https://doi.org/10.5194/egusphere-2026-5183
Preprint. Discussion started: 7 September 2026

During the preparation of this work, the main author used Claude Opus 4.6-4.8 to improve the clarity of selected author-written paragraphs and to optimise the performance of MATLAB scripts. After using this tool, the author reviewed and edited the content as needed and takes full responsibility for the content of the published article.

https://doi.org/10.5194/egusphere-2026-5183
Preprint. Discussion started: 7 September 2026

References

Andersen, O. G. N.: The annual cycle of temperature, salinity, currents and water masses in Disko Bugt and adjacent waters, West Greenland, Meddelelser om Grønland. Bioscience, 5, 1–33, https://doi.org/10.7146/mogbiosci.v5.142180, 1981.

Argo: Argo float data and metadata from Global Data Assembly Centre (Argo GDAC). [Data Set]., https://doi.org/10.17882/42182, (Accessed on 22-10-2024), 2026.

Beaird, N., Straneo, F., and Jenkins, W.: Characteristics of meltwater export from Jakobshavn Isbræ and Ilulissat Icefjord, Annals of Glaciology, 58, 107–117, https://doi.org/10.1017/aog.2017.19, 2017.

Burmeister, A.: The Fishery for Northern Shrimp (Pandalus borealis) off West Greenland, 1970–2025, NAFO Scientific Council Research Document SCR Doc. 25/038, 2025.

Cenedese, C. and Straneo, F.: Icebergs Melting, Annual Review of Fluid Mechanics, 55, 377–402, https://doi.org/10.1146/annurev-fluid-032522-100734, 2023.

CMEMS: Arctic Ocean Physics Reanalysis, https://doi.org/https://doi.org/10.48670/moi-00007, 2026a.

CMEMS: Global Ocean Physics Reanalysis, https://doi.org/https://doi.org/10.48670/moi-00021, 2026b.

CMEMS: Global Ocean Physics Analysis and Forecast, https://doi.org/https://doi.org/10.48670/moi-00016, 2026c.

Cuny, J., Rhines, P. B., and Ron Kwok: Davis Strait volume, freshwater and heat fluxes, Deep Sea Research Part I: Oceanographic Research Papers, 52, 519–542, https://doi.org/10.1016/j.dsr.2004.10.006, 2005.

Curry, B., Lee, C. M., and Petrie, B.: Volume, Freshwater, and Heat Fluxes through Davis Strait, 2004–05, Journal of Physical Oceanography, 41, 429–436, https://doi.org/10.1175/2010JPO4536.1, 2011.

Curry, B., Lee, C. M., Petrie, B., Moritz, R. E., and Kwok, R.: Multiyear Volume, Liquid Freshwater, and Sea Ice Transports through Davis Strait, 2004–10, Journal of Physical Oceanography, 44, 1244–1266, https://doi.org/10.1175/JPO-D-13-0177.1, 2014.

Dotto, T. S., Naveira Garabato, A., Bacon, S., Tsamados, M., Holland, P. R., Hooley, J., Frajka-Williams, E., Ridout, A., and Meredith, M. P.: Variability of the Ross Gyre, Southern Ocean: Drivers and Responses Revealed by Satellite Altimetry, Geophysical Research Letters, 45, 6195–6204, https://doi.org/10.1029/2018GL078607, 2018.

Dünweber, M., Swalethorp, R., Kjellerup, S., Nielsen, T. G., Arendt, K. E., Hjorth, M., Tönnesson, K., and Møller, E. F.: Succession and fate of the spring diatom bloom in Disko Bay, western Greenland, Marine Ecology Progress Series, 419, 11–29, https://doi.org/10.3354/meps08813, 2010.

Enderlin, E. M., Hamilton, G. S., Straneo, F., and Sutherland, D. A.: Iceberg meltwater fluxes dominate the freshwater budget in Greenland's iceberg-congested glacial fjords, Geophysical Research Letters, 43, 11,287–11,294, https://doi.org/10.1002/2016GL070718, 2016.

Foukal, N. P. and Pickart, R. S.: Moored Observations of the West Greenland Coastal Current along the Southwest Greenland Shelf, https://doi.org/10.1175/JPO-D-23-0104.1, 2023.

Gladish, C. V., Holland, D. M., and Lee, C. M.: Oceanic Boundary Conditions for Jakobshavn Glacier. Part II: Provenance and Sources of Variability of Disko Bay and Ilulissat Icefjord Waters, 1990-2011*, Journal of Physical Oceanography, 45, 33–63, https://doi.org/https://doi.org/10.1175/JPO-D-14-0045.1, 2015a.

Gladish, C. V., Holland, D. M., Rosing-Asvid, A., Behrens, J. W., and Boje, J.: Oceanic Boundary Conditions for Jakobshavn Glacier. Part I: Variability and Renewal of Ilulissat Icefjord Waters, 2001–14, Journal of Physical Oceanography, 45, 3–32, https://doi.org/10.1175/JPO-D-14-0044.1, 2015b.

Gou, R., Pennelly, C., and Myers, P. G.: The Changing Behavior of the West Greenland Current System in a Very High-Resolution Model, Journal of Geophysical Research: Oceans, 127, e2022JC018 404, https://doi.org/10.1029/2022JC018404, 2022.

Hamilton, L. C., Brown, B. C., and Rasmussen, R. O.: West Greenland's Cod-to-Shrimp Transition: Local Dimensions of Climatic Change, Arctic, 56, 271–282, https://www.jstor.org/stable/40512544, 2003.

Hansen, M. O., Nielsen, T. G., Stedmon, C. A., and Munk, P.: Oceanographic regime shift during 1997 in Disko Bay, Western Greenland, Limnology and Oceanography, 57, 634–644, https://www.jstor.org/stable/26954126, 2012.

Hersbach, H., Bell, B., Berrisford, P., Biavati, G., Horányi, A., Muñoz Sabater, J., Nicolas, J., Peubey, C., Radu, R., Rozum, I., Schepers, D., Simmons, A., Soci, C., Dee, D., and Thépaut, J-N.: ERA5 hourly data on single levels from 1940 to present. Copernicus Climate Change Service (C3S) Climate Data Store (CDS).[Data Set]., https://doi.org/10.24381/cds.adbb2d47, (Accessed on 20-11-2024), 2023.

Holland, D. M., Thomas, R. H., de Young, B., Ribergaard, M. H., and Lyberth, B.: Acceleration of Jakobshavn Isbræ triggered by warm subsurface ocean waters, Nature Geoscience, 1, 659–664, https://doi.org/10.1038/ngeo316, 2008.

Huang, J., Pickart, R. S., Bahr, F., McRaven, L. T., Tremblay, J.-, Michel, C., Jeansson, E., Kopec, B., Welker, J. M., and Ólafsdóttir, S. R.: Water mass evolution and general circulation of Baffin Bay: Observations from two shipboard surveys in 2021, Progress in Oceanography, p. 103322, https://doi.org/10.1016/j.pocean.2024.103322, 2024.

Huang, J., Pickart, R., Spall, M., Myers, P., Bahr, F., Kopec, B., Jeansson, E., and Welker, J.: Shelf–Fjord Exchange Regulated by Recirculating Greenland Meltwater in Glacial Troughs, https://doi.org/10.21203/rs.3.rs-7321564/v1, 2025.

Huang, J., Pickart, R. S., and Pacini, A.: Wind-Driven Downwelling Along the West Greenland Shelf and Slope From 6 Years of Mooring Data, Journal of Geophysical Research: Oceans, 131, e2025JC022 873, https://doi.org/10.1029/2025JC022873, 2026.

IAPB: Disko Bay 2025. [Data Set]., https://iabp.apl.uw.edu/DiskoBay_2025.html, 2025.

Jean-Michel, L., Eric, G., Romain, B.-B., Gilles, G., Angélique, M., Marie, D., Clément, B., Mathieu, H., Olivier, L. G., Charly, R., Tony, C., Charles-Emmanuel, T., Florent, G., Giovanni, R., Mounir, B., Yann, D., and Pierre-Yves, L. T.: The Copernicus Global 1/12° Oceanic and Sea Ice GLORYS12 Reanalysis, Frontiers in Earth Science, 9, https://doi.org/10.3389/feart.2021.698876, 2021.

Johns, W. E., Baringer, M. O., Beal, L. M., Cunningham, S. A., Kanzow, T., Bryden, H. L., Hirschi, J. J. M., Marotzke, J., Meinen, C. S., Shaw, B., and Curry, R.: Continuous, Array-Based Estimates of Atlantic Ocean Heat Transport at 26.5°N, Journal of Climate, 24, 2429–2449, https://doi.org/10.1175/2010JCLI3997.1, 2011.

Joughin, I., Abdalati, W., and Fahnestock, M.: Large fluctuations in speed on Greenland's Jakobshavn Isbræ glacier, Nature, 432, 608–610, https://doi.org/10.1038/nature03130, 2004.

Joughin, I., Shean, D. E., Smith, B. E., and Floricioiu, D.: A decade of variability on Jakobshavn Isbræ: ocean temperatures pace speed through influence on mélange rigidity, The Cryosphere, 14, 211–227, https://doi.org/10.5194/tc-14-211-2020, 2020.

Kaihatu, J. M., Handler, R. A., Marmorino, G. O., and Shay, L. K.: Empirical Orthogonal Function Analysis of Ocean Surface Currents Using Complex and Real-Vector Methods, Journal of Atmospheric and Oceanic Technology, 15, 927–941, https://doi.org/10.1175/1520-0426(1998)015<0927:EOFAOO>2.0.CO;2, 1998.

Kajanto, K., Straneo, F., and Nisancioglu, K.: Impact of icebergs on the seasonal submarine melt of Sermeq Kujalleq, The Cryosphere, 17, 371–390, https://doi.org/10.5194/tc-17-371-2023, 2023.

Khazendar, A., Fenty, I. G., Carroll, D., Gardner, A., Lee, C. M., Fukumori, I., Wang, O., Zhang, H., Seroussi, H., Moller, D., Noël, B. P. Y., van den Broeke, M. R., Dinardo, S., and Willis, J.: Interruption of two decades of Jakobshavn Isbrae acceleration and thinning as regional ocean cools, Nature Geoscience, 12, 277–283, https://doi.org/10.1038/s41561-019-0329-3, 2019.

Kiilerich, A.: The Hydrography of the West Greenland Fishing Banks, Meddelelser fra Kommissionen for Danmarks Fiskeri- og Havundersøgelser, 11, 1943.

Krawczyk, D. W., Vonnahme, T., Burmeister, A. D., Maier, S. R., Blicher, M. E., Meire, L., and Nygaard, R.: Arctic puzzle: Pioneering a northern shrimp (*Pandalus borealis*) habitat model in Disko Bay, West Greenland, Science of The Total Environment, 929, 172 431, https://doi.org/10.1016/j.scitotenv.2024.172431, 2024.

Latuta, L., Smedsrud, L. H., Darelius, E., Hansen, P. J., and Willis, J. K.: Drivers of seasonal hydrography in Disko Bay, Greenland, Ocean Science, 21, 3487–3505, https://doi.org/10.5194/os-21-3487-2025, 2025.

Le Corre, N., Pepin, P., Burmeister, A., Walkusz, W., Skanes, K., Wang, Z., Brickman, D., and Snelgrove, P. V.: Larval connectivity of northern shrimp (Pandalus borealis) in the Northwest Atlantic, Canadian Journal of Fisheries and Aquatic Sciences, 77, 1332–1347, https://doi.org/10.1139/cjfas-2019-0454, 2020.

Lee, C.: Davis Strait hydrographic mooring Level 2 data: temperature, salinity, and velocity measurements from the Davis Strait Observing System moorings, 2004 to 2022. [Data Set], https://doi.org/10.18739/A2416T169, 2024.

Lenetsky, J. E.: Variability and impacts of present and future oceanic exchanges in Baffin Bay, PhD thesis, University of Colorado, Boulder, Colorado, USA, https://doi.org/10.5065/D6RX99HX, 2026.

Marmorino, G. O., Shay, L. K., Haus, B. K., Handler, R. A., Graber, H. C., and Horne, M. P.: An EOF analysis of HF Doppler radar current measurements of the Chesapeake Bay buoyant outflow, Continental Shelf Research, 19, 271–288, https://doi.org/10.1016/S0278-4343(98)00078-8, 1999.

Meire, L., Mortensen, J., Meire, P., Juul-Pedersen, T., Sejr, M. K., Rysgaard, S., Nygaard, R., Huybrechts, P., and Meysman, F. J. R.: Marine-terminating glaciers sustain high productivity in Greenland fjords, Global Change Biology, 23, 5344–5357, https://doi.org/10.1111/gcb.13801, 2017.

Mernild, S. H., Holland, D. M., Holland, D., Rosing-Asvid, A., Yde, J. C., Liston, G. E., and Steffen, K.: Freshwater Flux and Spatiotemporal Simulated Runoff Variability into Ilulissat Icefjord, West Greenland, Linked to Salinity and Temperature Observations near Tidewater Glacier Margins Obtained Using Instrumented Ringed Seals, Journal of Physical Oceanography, 45, 1426–1445, https://doi.org/10.1175/JPO-D-14-0217.1, 2015.

Motyka, R. J., Truffer, M., Fahnestock, M., Mortensen, J., Rysgaard, S., and Howat, I.: Submarine melting of the 1985 Jakobshavn Isbræ floating tongue and the triggering of the current retreat, Journal of Geophysical Research: Earth Surface, 116, https://doi.org/10.1029/2009JF001632, 2011.

Myers, P. G., Castro de la Guardia, L., Fu, C., Gillard, L. C., Grivault, N., Hu, X., Lee, C. M., Moore, G. W. K., Pennelly, C., Ribergaard, M. H., and Romanski, J.: Extreme High Greenland Blocking Index Leads to the Reversal of Davis and Nares Strait Net Transport Toward the Arctic Ocean, Geophysical Research Letters, 48, e2021GL094 178, https://doi.org/10.1029/2021GL094178, 2021.

Møller, E. F., Christensen, A., Larsen, J., Mankoff, K. D., Ribergaard, M. H., Sejr, M., Wallhead, P., and Maar, M.: The sensitivity of primary productivity in Disko Bay, a coastal Arctic ecosystem, to changes in freshwater discharge and sea ice cover, Ocean Science, 19, 403–420, https://doi.org/10.5194/os-19-403-2023, 2023.

Münchow, A., Falkner, K. K., and Melling, H.: Baffin Island and West Greenland Current Systems in northern Baffin Bay, Progress in Oceanography, 132, 305–317, https://doi.org/10.1016/j.pocean.2014.04.001, 2015.

Nelson, M., Straneo, F., Purkey, S. G., Waterhouse, A. F., Fogaren, K. E., and Torres, D. J.: Observations of Water Mass Modification and Cross-Shelf Exchange at Narsaq Trough, Greenland, Journal of Geophysical Research: Oceans, 130, e2024JC022 246, https://doi.org/10.1029/2024JC022246, 2025.

https://doi.org/10.5194/egusphere-2026-5183
Preprint. Discussion started: 7 September 2026

Nielsen, J.: The Waters round Greenland, in: Greenland, vol. 1, pp. 185–230, Copenhagen / London, 1928.

NOAA National Geophysical Data Center: ETOPO1 1 Arc-Minute Global Relief Model. [Data Set], 2009.

North, G. R., Bell, T. L., Cahalan, R. F., and Moeng, F. J.: Sampling Errors in the Estimation of Empirical Orthogonal Functions, Monthly Weather Review, 110, 699–706, https://doi.org/10.1175/1520-0493(1982)110<0699:SEITEO>2.0.CO;2, 1982.

Oliver, H., Slater, D., Carroll, D., Wood, M., Morlighem, M., and Hopwood, M. J.: Greenland Subglacial Discharge as a Driver of Hotspots of Increasing Coastal Chlorophyll Since the Early 2000s, Geophysical Research Letters, 50, e2022GL102 689, https://doi.org/10.1029/2022GL102689, 2023.

Pacini, A. and Pickart, R. S.: Wind-Forced Upwelling Along the West Greenland Shelfbreak: Implications for Labrador Sea Water Formation, Journal of Geophysical Research: Oceans, 128, e2022JC018 952, https://doi.org/10.1029/2022JC018952, 2023.

Pacini, A., Pickart, R. S., Bahr, F., Torres, D. J., Ramsey, A. L., Holte, J., Karstensen, J., Oltmanns, M., Straneo, F., Bras, I. A. L., Moore, G. W. K., and Jong, M. F. d.: Mean Conditions and Seasonality of the West Greenland Boundary Current System near Cape Farewell, Journal of Physical Oceanography, 50, 2849–2871, https://doi.org/10.1175/JPO-D-20-0086.1, 2020.

Picton, H. J., Nienow, P. W., Slater, D. A., and Chudley, T. R.: A Reassessment of the Role of Atmospheric and Oceanic Forcing on Ice Dynamics at Jakobshavn Isbræ (Sermeq Kujalleq), Ilulissat Icefjord, Journal of Geophysical Research: Earth Surface, 130, e2024JF008 104, https://doi.org/10.1029/2024JF008104, 2025.

Schauer, U. and Beszczynska-Möller, A.: Problems with estimation and interpretation of oceanic heat transport – conceptual remarks for the case of Fram Strait in the Arctic Ocean, Ocean Science, 5, 487–494, https://doi.org/10.5194/os-5-487-2009, 2009.

Schiller-Weiss, I., Martin, T., and Schwarzkopf, F. U.: Emerging Influence of Enhanced Greenland Melting on Boundary Currents and Deep Convection Regimes in the Labrador and Irminger Seas, Geophysical Research Letters, 51, e2024GL109 022, https://doi.org/10.1029/2024GL109022, 2024.

Shan, X., Spall, M. A., Pennelly, C., and Myers, P. G.: Seasonal Variability in Baffin Bay, Journal of Geophysical Research: Oceans, 129, e2024JC021 038, https://doi.org/10.1029/2024JC021038, 2024.

Smith, E., Soule, F., and Mosby, O.: The "Marion" and "General Greene" Expeditions to Davis Strait and Labrador Sea; under the direction of the U.S. Coast Guard, 1928-1931-1933-1934-1935. Scientific results pt. 2: Physical Oceanography., 19, 1937.

Tang, C. C. L., Ross, C. K., Yao, T., Petrie, B., DeTracey, B. M., and Dunlap, E.: The circulation, water masses and sea-ice of Baffin Bay, Progress in Oceanography, 63, 183–228, https://doi.org/10.1016/j.pocean.2004.09.005, 2004.

Tschudi, M., Meier, W., Stewart, J., Fowler, C., and Maslanik, J.: Polar Pathfinder Daily 25 km EASE-Grid Sea Ice Motion Vectors, Version 4, https://doi.org/10.5067/INAWUWO7QH7B, 2019.

Wood, M., Carroll, D., Fenty, I., Bertin, C., Darby, B., Dutkiewicz, S., Hopwood, M., Khazendar, A., Meire, L., Oliver, H., Parker, T., and Willis, J.: Increased melt from Greenland's most active glacier fuels enhanced coastal productivity, Communications Earth & Environment, 6, 626, https://doi.org/10.1038/s43247-025-02599-1, 2025.